Revision 2

Synthesis and characterization of amphiboles along the tremolite–glaucophane join

by

David M. Jenkins[1], Giancarlo Della Ventura[2], Roberta Oberti[3], Krassimir Bozhilov[4]

[1]Department of Geological Sciences and Environmental Studies, Binghamton University, Binghamton, NY, 13902-6000, U.S.A.

[2]Dipartimento di Scienze Geologiche, Università di Roma Tre, Largo S. Leonardo Murialdo, 1 I-00146, Italy

[3]CNR-Istituto di Geoscienze e Georisorse, Unità di Pavia, via Ferrata, 1 I-27100 Pavia, Italy

[4]Department of Earth Sciences, University of California, Riverside, CA 92521, U.S.A.

Abstract

Actinolite and glaucophane are the principal amphiboles in greenschist- and blueschist-facies metamafic rocks, respectively, and constitute an important mineral pair for deducing the conditions of medium- and high-pressure metamorphism. Here we present the crystal-chemical properties of amphiboles synthesized long the tremolite–glaucophane join as an important starting point for the more chemically complex samples occurring in nature. Amphiboles were synthesized in 10 mole% increments at conditions ranging from 840°C and 0.6 GPa for tremolite-rich to 750°C and 2.5 GPa for glaucophane-rich amphiboles. The amphibole yields were generally high (~95 wt%), though minor quartz, pyroxene, and amorphous material (either glass or quenched solute) were often present. Electron microprobe analysis of the amphibole showed that deviations from the nominal or intended compositions occurred, with the observed compositions showing solid solution primarily toward the katophorite component and reaching a

maximum near the middle of the join. Unit-cell dimensions showed a pronounced positive deviation from ideality, even after (linear) correction for the non-join components, suggesting a strong tendency toward exsolution. Single-crystal refinements of a couple of selected amphiboles confirmed the deviation from nominal composition and confirmed the presence of ^{A}Na, ^{T}Al, and ^{C}Al, the latter disordered between the *M*(2) and *M*(3) sites. Infrared spectra in the OH-stretching region were measured on samples that were heated to 250-350°C to remove absorbed moisture. The spectra consist of a main band centered in the 3675-3660 cm^{-1} region and two minor absorptions on both sides of the dominant central peak, which are centered at 3720 and 3640 cm^{-1} and can be attributed to OH next to ^{A}Na and ^{C}Al, respectively. The main band is evidently composed of several overlapping components due to local arrangements of B cations typical of tremolite, CaCa, glaucophane, NaNa, and cummingtonite, MgMg. Examination of several intermediate amphiboles by both single-crystal XRD and by high-resolution TEM analysis could not identify evidence of reflections or ordered domains that would violate the *C*2/*m* symmetry of the end-member amphiboles. Comparing the compositions of the synthetic amphiboles from this study with winchite-rich amphiboles in nature shows that deviations from the tremolite–glaucophane join are common. The inability to make pure winchite or even winchite-rich amphiboles on the tremolite–glaucophane join suggests that this structure is unstable.

Keywords: glaucophane, tremolite, winchite, katophorite, high-pressure metamorphism, unit-cell dimensions, short-range order, HRTEM, FTIR

Introduction

Glaucophane, $\square Na_2Mg_3Al_2Si_8O_{22}(OH)_2$ (= Gl, where $\square$ represents a vacancy), is the key index mineral of mafic rocks metamorphosed to the blueschist facies. Experimental studies on end-member glaucophane have proven difficult in the past because of the formation of a sodium-rich sheet silicate and because of deviations from its ideal stoichiometry (e.g., Ernst, 1961; Ernst, 1963; Maresch, 1977; Koons, 1982; Carman and Gilbert, 1983; Pawley, 1992; Welch and Graham, 1992; Tropper et al., 2000). More recently, Jenkins and Corona (2006a), Corona and Jenkins (2007), Jenkins (2011), and Basora et al. (2012) have demonstrated that essentially pure glaucophane can be synthesized if strict control is maintained on the water content during its synthesis to prevent the nucleation of a sheet silicate (variably identified as smectite or vermiculite) and to minimize the loss of more soluble constituents (Si, Na, and Al) to the ambient solution, both of which can drive the resultant amphibole away from end-member glaucophane. This has allowed some key reactions to be investigated that define the *P*-*T* stability field of glaucophane. In this study, the crystal-chemical relations between glaucophane and tremolite ($\square Ca_2Mg_5Si_8O_{22}(OH)_2$ = Tr) are investigated. Solid solution between these end members provides important insights into, for example, compositional changes occurring in amphiboles subjected to conditions typical for blueschist- to greenschist-facies rocks. In this paper, we use the amphibole formulae and terminology proposed in the newly approved scheme for amphibole classification and nomenclature (Hawthorne et al., 2012), i.e., $A_{0\text{-}1}B_2C_5T_8O_{22}W_2$, where $^{VI\text{-}X}A$, $^{VI\text{-}VIII}B$, ^{VI}C, ^{IV}T and $^{II\text{-}III}W$ are mixtures of ions of different charges occurring at the relevant group of crystallographic sites, and end-member compositions are defined based on distinct arrangements of dominant charges. Also, the new rules imply that the names of the sites for monoclinic amphiboles have italicized letters and specifications between parentheses.

Previous experimental studies on tremolite and glaucophane have shown that amphiboles made along a given compositional join may deviate noticeably from their intended compositions. For example, Graham et al. (1989) and Pawley et al. (1993) studied the join tremolite–richterite ($Na(CaNa)Mg_5Si_8O_{22}(OH)_2$) and found a systematic deviation toward enrichment in cummingtonite ($\square Mg_2Mg_5Si_8O_{22}(OH)_2$ = Cm) with increasing Tr content. This was one of the first joins where deviations in amphibole solid-solution compositions were confirmed by direct electron microprobe analysis. Similar behavior was observed for amphiboles made along the join tremolite–tschermakite ($\square Ca_2(Mg_3Al_2)(Al_2Si_6)O_{22}(OH)_2$; Cho and Ernst, 1991; Smelik et al., 1994) tremolite–pargasite ($NaCa_2(Mg_4Al)(Al_2Si_6)O_{22}(OH)_2$; Sharma and Jenkins, 1999) and richterite–pargasite (Della Ventura et al., 1999). Pawley (1992) found that amphiboles made along the join glaucophane–nybøite ($Na(Na_2)(Mg_3Al_2)(AlSi_7)O_{22}(OH)_2$ = Ny) were displaced toward ^{B}Mg-substituted katophorite ($Na(NaMg)(Mg_4Al)(AlSi_7)O_{22}(OH)_2$ = ^{B}Mg-Kt) and were buffered to the three-component system Gl–Ny–^{B}Mg-Kt in the presence of quartz. Tropper et al (2000) studied compositional variations in glaucophane equilibrated with jadeite and talc and observed that the amphibole deviated primarily toward enrichment in the Ny and Cm components. In their attempts to synthesize magnesio-riebeckite ($\square Na_2(Mg_3Fe^{3+}_2)Si_8O_{22}(OH)_2$), Della Ventura et al. (2005) observed that the resultant amphibole had a composition essentially along the join magnesio-riebeckite–magnesio-arfvedsonite ($NaNa_2(Mg_4Fe^{3+})Si_8O_{22}(OH)_2$), while Iezzi et al. (2004a) explored the effect of varying f_{O2} on the synthesis of ferri-clinoholmquistite, ideally $\square Li_2(Mg_3Fe^{3+}_2)Si_8O_{22}(OH)_2$, and observed significant deviation related to the $^{M(2)}(Mg,Fe^{2+})$ $^{M(4)}(Mg,Fe^{2+})$ $^{M(2)}Fe^{3+}_{-1}$ $^{M(4)}Li_{-1}$ exchange vector. It is evident from these studies that amphibole compositions frequently do not conform to a proposed compositional join and

that it is important to quantify the presence and extent of any compositional deviations that might exist.

It is well known from detailed studies of metamorphic amphiboles (e.g., Himmelberg and Papike, 1969; Maresch et al., 1982; Reynard and Ballèvre, 1988; Smelik and Veblen, 1992; Schumacher, 2007) that glaucophane frequently shares a miscibility gap, rather than complete solid solution, with calcic amphiboles. This indicates a positive deviation from ideal mixing which is usually apparent as an excess volume of mixing, as seen, for example, along the alkali-feldspar join (Hovis and Graeme-Barber, 1997; Hovis et al., 1999). Accordingly, it is important to examine the volume-composition relationships for the tremolite–glaucophane join as part of the larger task of understanding the cation mixing behavior of these end-member components.

Cation order, particularly near the middle of this join, should be considered as well. Though certainly not identical structurally, the chemically-related diopside–jadeite pyroxene join undergoes a change from *C*2/*c* to *P*2/*n* symmetry for omphacite near the middle of this join caused by ordering of Mg, Al, Ca, and Na at crystallographically independent sites, which has been discussed in earlier studies (e.g., Carpenter, 1979; 1981; Holland, 1983; Nakamura and Banno, 1997; Boffa Ballaran et al., 1998; Pavese et al., 2000; Green et al., 2007; Müller and Compagnoni, 2009). In monoclinic amphiboles, a lowering in symmetry to $P2_1/m$ related to cation order is known in cummingtonite and in ^{B}(NaMg) amphiboles, where it occurs only where the Na:Mg ratio is close to 1:1. Indeed, the occurrence of small B cations or of 1:1 alternating small ($^{[8]}$Mg, i.r. = 0.89 Å) and large ($^{[8]}$Na, i.r. = 1.18 Å) B cations strongly affects the conformation of the double chain of tetrahedra as well, a feature which is allowed by $P2_1/m$ symmetry (Cámara et al., 2003; Iezzi et al., 2004b); in contrast, no further order is possible in this space group for C cations beyond that commonly observed in the amphibole supergroup

(high-charge cations order at *M*(2) but for partly or totally dehydrogenated compositions). Indeed, single-crystal X-ray refinement (SREF) of winchite-like compositions (e.g., Ghose et al., 1986; Sokolova et al., 2001) and other sodium-calcium amphiboles has never revealed anything other than *C*2/*m* symmetry. However, the presence of small domains with $^{B}Mg_2$ or ^{B}(NaMg) and $P2_1/m$ symmetry might cause deviations from stoichiometry. This issue was carefully investigated for amphiboles made near the middle of the join in this work.

Short-range order was examined using infrared (IR) spectroscopy near the OH-stretching region. There has been extensive work on the IR spectra of synthetic amphiboles over the past several decades, as reviewed by Hawthorne and Della Ventura (2007), devoted to determining the correlation between specific schemes of cation order and the observed bands in the OH-stretching region. The IR spectra can also be used to independently determine the presence of ^{A}Na (e.g. Rowbotham and Farmer, 1974, Hawthorne et al., 1997).

Methods

Amphibole synthesis and apparatus

All amphiboles were synthesized from reagent grade oxides and carbonates. The source of SiO_2 was desiccated silicic acid, heated in steps to a maximum temperature of 1100°C and yielding amorphous silica or weakly crystalline cristobalite. Aluminum was added in the form of Al_2O_3 while Mg was added in the form of MgO for most of the starting mixtures, though for some (TREM 26, WIN 13, and FEGL 5) $Mg(OH)_2$ was used because it tended to give a higher initial yield of amphibole for Gl-rich bulk compositions. Sodium was added as Na_2CO_3 while for most mixtures Ca was added as $CaCO_3$. For one mixture (TREM 26) Ca was added as $Ca(OH)_2$ to see if any improvement in amphibole yield could be obtained. Starting mixtures prepared with carbonates were decarbonated by heating in air at 900°C for 15 minutes, which

was sufficient to remove CO_2 by reaction with silica. Addition of any hydroxide ($Mg(OH)_2$ or $Ca(OH)_2$) was done after decarbonation. The bulk compositions of all mixtures investigated in this study are listed in Table 1.

Syntheses were done by sealing portions of the starting mixtures along with specific weight percentages of distilled water, or simply as a dry mixture if excess water was present in a hydroxide reagent, in Pt capsules that were either 4 mm outer diameter (OD) by 15 mm length or 5 mm OD by 18 mm length having wall thicknesses of 0.13-0.18 mm. Capsule treatments in the 0.45-0.63 GPa range were done in internally-heated gas vessels using Ar as the pressure medium and using two Inconel®-sheathed chromel-alumel thermocouples situated across the length of the capsule to monitor the temperature and thermal gradient across the capsule length. Additional details of this apparatus are given in Lledo and Jenkins (2008). Capsule treatments in the 1.5-2.5 GPa range were done in a ½-inch diameter piston-cylinder press using NaCl as the pressure medium and fitted with a straight graphite furnace. Pressure calibration of this assemblage was reported in Quirion and Jenkins (1998). Temperatures were monitored and controlled with a chromel-alumel thermocouple positioned directly above the sample. The specific treatment conditions and weight percentages of water used in the treatment are listed in Table 2.

Analytical equipment and methods

Powder X-ray diffraction analysis and Rietveld structure refinements were done at Binghamton University using a Philips Xpert PW3040-MPD diffractometer operated at 40 kV and 20 mA using Cu-Kα radiation and fitted with a diffracted-beam graphite monochromator. The powdered samples were mounted on zero-background oriented quartz plates and scanned from 8 to 100° 2θ with step sizes of 0.05° 2θ for durations sufficient to obtain 2000 counts on the

strongest peaks. Rietveld refinements were done using the program GSAS (Larson and Von Dreele, 2000) and initiating the refinements by using the structures of tremolite from Hawthorne and Grundy (1976), winchite from Sokolova et al. (2001), glaucophane from Papike and Clark (1968), katophorite ($Na(NaCa)(Mg_4Al)(AlSi_7)O_{22}(OH)_2$ = Kt) from Hawthorne et al. (2006), quartz from Levien et al. (1980), enstatite from Nestola et al. (2006), talc from Perdikatsis and Burzlaff (1981), diopside from Levien and Prewitt (1981), omphacite (*P*2/*n*) from Pavese et al. (2000), and jadeite from Prewitt and Burnham (1966). The refinements were started by refining the zeropoint using the quartz in the pattern, if present, as an internal standard, followed by adding the remaining parameters, including the background, profile parameters, cell dimensions, atom coordinates, etc. using the full data set (0.05° 2θ step size). This tended to yield low Durbin-Watson *d* statistics (0.7-1.2) indicating a high amount of serial correlation and artificially low uncertainties (Hill and Flack, 1987). Therefore, a second refinement was done on the same pattern but with every other data point filtered (an effective 0.10° 2θ step size) and holding all variables constant except the background and unit-cell dimensions. This produced improved Durbin-Watson *d* statistics (0.8-1.9) with correspondingly larger uncertainties, both of which are reported here, and without significantly different unit-cell dimensions. It is emphasized that this second refinement was done only to provide better estimates of the uncertainties in the cell dimensions; the cell dimensions reported here are based on the full (0.05° 2θ step size) data set.

Electron microprobe (EMP) analysis was done on a JEOL 8900 Superprobe using samples mounted in epoxy and polished to 0.5 μm diamond grit size. Operating conditions for all analyses were 15 kV and 10 nA using albite as the standard for Na, diopside for Ca, and the pure oxides for Mg, Al, and Si. Matrix corrections were made with the ZAF scheme. Sodium X-ray counts were monitored for the glaucophane-rich amphiboles made in this study to check for the

183 extent of Na diffusion under the electron beam, but none was observed for counting durations of
184 1 minute in spot mode (~ 1 μm diameter). Even so, the counting times for WDS analyses were
185 kept to 10 s on the peak and 3 s on the background to minimize Na diffusion from either the
186 albite standard or the sample.

187 Single-crystal X-ray diffraction refinement (SREF) and crystal-chemical analysis were done
188 for samples WIN 4-2 and WIN 9-1, the only samples where crystal size (65 x 15 x 8 and 50 x 10
189 x 10 μm, respectively, for the analyzed crystals) allowed collection of good quality data. Data
190 collection was done at CNR-IGG in Pavia, Italy, using a Bruker-AXS Smart-Apex CCD-based
191 diffractometer equipped with graphite-monochromatized Mo-Kα X-radiation. Omega-rotation
192 frames (scan width 0.2°, scan time 50 s, sample-to detector distance 50 mm) were processed with
193 the SAINT software (Bruker®, 2003) and intensities were corrected for Lorentz and polarization
194 effects; absorption effects were empirically evaluated by the SADABS software (Sheldrick,
195 1996) and an absorption correction was applied to the data. Accurate unit-cell dimensions were
196 calculated by least-squares refinement of the positions of 836 independent reflections with $I >$
197 $10\sigma(I)$ in the θ range 2-30°.

198 FTIR powder spectra were obtained at INFN (Istituto Nazionale di Fisica Nucleare, Frascati,
199 Rome) using a Bruker Hyperion 3000 FTIR microscope equipped with a N_2-cooled MCT
200 detector, a KBr beamsplitter and a Globar source. Samples were prepared as KBr pellets, with a
201 mineral:KBr ratio = 5:150 mg. A Linkam FTIR600 heating/freezing stage was used for high-
202 temperature data collection, at 4 cm^{-1} nominal resolution, accumulating 256 patterns both on the
203 peak and on the background.

204 Transmission electron microscopy (TEM) was done at the University of California at
205 Riverside with a FEI-Philips CM300 microscope operating at 300 kV accelerating voltage,

206 equipped with a LaB_6 electron gun, and an EDAX energy-dispersive spectrometer (EDS).
207 Samples were prepared by dispersing the unground crystal aggregates in distilled water through
208 ultrasonic agitation and depositing a drop of the resulting suspension onto copper grids coated
209 with a thin (5 nm thickness) holey carbon support film. Selected-area and convergent beam
210 electron diffraction (SAED and CBED) patterns and high-resolution images were obtained
211 typically along the [100] and [U0W] zone axes of individual amphibole crystals.

212 **Results**

213 **Optimization of amphibole yield**

214 A series of reconnaissance experiments was done over the range of 750-850°C and 1.5-2.5 GPa
215 using mixtures that were made on, and slightly off of, the tremolite–glaucophane join (i.e., WIN
216 3, WIN 4) to determine what conditions were optimum for amphibole synthesis. Bulk
217 compositions that were slightly off of the join involved a Tr-rich end-member composition that
218 was purposely shifted by 5-10 mol% enrichment in the Cm component for reasons that were
219 reviewed by Bozhilov et al. (2007). In general, the amphibole yields were high (~ 95 wt%) as
220 can be seen in the back-scattered electron images of representative samples shown in Figure 1.
221 Unfortunately, there were no specific pressure-temperature (*P*-*T*) conditions that produced pure
222 yields of amphibole. Usually the synthesis products consisted of amphibole coexisting with
223 quartz as the most abundant additional phase, though minor (1-5 wt %) or trace (< 1 wt%)
224 amounts of a pyroxene were formed at higher temperatures or talc at lower temperatures. An
225 amorphous phase was observed to occur interstitial to the amphibole crystals, seen as the darker-
226 grey matrix material in Figure 1c, for bulk compositions near the middle of the join. It is not
227 clear if this material is a quenched silicate melt or if it is a solute that precipitates upon quench.
228 It is suspected that the latter case is a more likely explanation, as this material either appears or

increases in abundance with multiple treatments at the same *P-T* conditions, as shown, for example, by samples WIN 1-1 and WIN 1-2 in Table 2, whose XRD patterns are shown in Figures 2a,b. The pattern in Figure 2b (second treatment) shows a distinct drop in the intensity of the quartz peak at 26.6° 2θ compared to Figure 2a (first treatment) and a concomitant appearance of a broad diffraction maximum centered at about 17.5° 2θ that is attributed to the amorphous material, though this maximum is lower than that observed in Mg-silicate glasses (Thompson, 2008) or soda-lime-silicate glass (e.g., Abo-Mosallam et al., 2010). In general, the highest amphibole yields were obtained by treating mixtures at conditions that varied between 840°C and 0.6 GPa for the Tr-rich compositions and 750°C and 2.5 GPa for Gl-rich compositions. These conditions are listed in Table 2.

Amphibole compositions

Electron microprobe analyses of amphiboles formed in this study are listed in Table 3. It should be noted that analysis of small amphibole grains often leads to low analytical totals; however, grains with analytical totals ≥ 70 wt% generally give cation proportions that are the same, within analytical precision, as those of the bulk sample as demonstrated, for example, by Jenkins and Corona (2006a). The amphibole compositions are plotted in Figure 3a, which is a projection from H_2O onto the $(NaAl)O_2$-CaO-MgO-SiO_2 quadrilateral. Also shown in Figure 3a is a sub-tetrahedron defined by the ideal compositions tremolite–glaucophane–cummingtonite–katophorite which encompasses the amphiboles formed in this study. Although not always obvious when viewing the quadrilateral in Figure 3a from different vantage points, there is a systematic deviation in the observed compositions from the nominal or expected compositions along the tremolite–glaucophane join. This is more apparent when amphibole compositions are projected from H_2O and cummingtonite onto the $(NaAl)O_2$-CaO-SiO_2 ternary (Figure 3b). Here

the observed compositions (open circles, amph) are displaced away from the SiO_2 apex near the middle of the join toward the katophorite bulk composition. This explains the persistent coexistence of quartz in the synthesis products. The strong correlation between Na and Al can be seen in Figures 4a,b. Figure 4a shows ^{A}Na versus ^{T}Al, while Figure 4b shows ^{B}Na versus ^{C}Al. In both cases they closely follow the ideal trends for the tremolite–katophorite and tremolite–glaucophane joins, respectively. Note that the correlations observed in this figure result from the conventional site partitioning used for amphiboles (e.g., Leake et al., 1997) and are independent of any choice of components used to represent the amphibole compositions. This plot also provides some justification for showing Na and Al as the combined components in the ternary projection in Figure 3b.

Varying the temperature of synthesis from 760-820°C, as was done for the WIN 11-1, -2, -3, and -4 samples in Table 2, does not affect the resultant composition in any significant manner, as seen by the grey circles in Figure 3b. It should also be noted that the quenched amorphous material (grey squares, Fig. 3b) formed in the WIN 11-series syntheses plots near the SiO_2–$(NaAl)O_2$ join and is in approximate mass balance with the coexisting amphiboles (± quartz) for the WIN 11 bulk composition (grey triangle).

Unit-cell dimensions

The unit-cell dimensions for selected amphiboles from Table 3 were determined from Rietveld refinements of the powder X-ray diffraction patterns and are listed in Table 4. These are plotted in Figure 5a as a function of the mole fraction of ^{B}Ca. The dashed line represents ideal mixing between pure glaucophane (863Å^3; Jenkins and Corona, 2006b) and tremolite (907Å^3; Yang and Evans, 1996), while the curve is a polynomial fit to the data constrained to pass through the end-member volumes. This curve adequately represents all but the most Ca-rich samples which,

because of the presence of ^{B}Mg that is always observed (e.g., Yang and Evans, 1996), have smaller volumes than expected. Owing to the solid solution present in these samples, a correction was applied to the observed volumes to compensate for the Cm and Kt components. Table 5 reports the compositions of selected amphiboles after recasting them into the mole fractions of Tr, Gl, Cm, and Kt (or Ny) components as indicated in the footnote to Table 5. One can then calculate a corrected unit-cell volume (V_{corr}) for the Cm, Kt, or Ny components as follows:

$$V_{corr} = [V_{obs} - (X_{Cm} \cdot V_{Cm} + X_{Kt} \cdot V_{Kt} + X_{Ny} \cdot V_{Ny})]/(X_{Tr} + X_{Gl}) \quad (1)$$

where V_{obs} is the observed volume, X_i is the mole fraction of component i, and V_i is the volume of pure component i. The unit-cell volumes adopted for this study are V_{Cm} = 874.4 Å^3 (extrapolated from heated - *C*2/*m* - samples in the cummingtonite-grunerite join; Hirschmann et al., 1994), V_{Kt} = 893.1 Å^3 (this study), and V_{Ny} = 871.5 Å^3 (extracted from the CNR-IGG-PV amphibole database based on an updated version of the procedure reported by Hawthorne and Oberti, 2007). It should be noted that the V_{Kt} observed in this study is very close to the volume of 892.8 Å^3 extracted from the CNR-IGG-PV amphibole database. The corrected volumes are given in Table 5. Figure 5b shows the values of V_{corr} plotted against Tr', which is the mole fraction of Tr in the amphibole projected onto the binary join glaucophane–tremolite (i.e., excluding Cm, Kt, and Ny components). Although the individual samples have large uncertainties, it is apparent that the overall V_{corr}-composition dependence is essentially the same as that in Figure 5a and is well modeled by the same polynomial curve. The underlying assumption behind equation (1) is that volume corrections over compositional ranges up to ~35% are linear. There is no particular reason to expect such close agreement in the volume-composition relations between the observed and corrected volumes, which suggests that the

dominant factor controlling the deviation from ideal mixing along this join is caused by the excess volume of mixing between the Gl and Tr components in these amphiboles.

Single-crystal refinement and crystal-chemical analysis

Because crystals formed near the middle of the join were relatively larger than elsewhere along the join (Fig. 1b), it was possible to obtain a single-crystal refinement of two of the amphiboles formed here. Reflections with $I_o > 3\ \sigma(I)$ were considered as observed during unweighted full-matrix least-squares refinement on F done using a program specifically written at CNR-IGG-Pavia to deal with complex solid-solutions. Scattering curves for fully ionized scattering species were used at sites where chemical substitutions occur; neutral vs. ionized scattering curves were used at the T and anion sites. The resulting R_{obs} factors are 4.4% (to $\theta = 35°$) and 3.5% (to $\theta = 30°$) for samples WIN 4-2 and WIN 9-1, respectively. Relevant crystallographic results have been deposited as supplementary material (Table 6).

Comparison of refined mean-bond lengths and site-scattering values based on the present crystal-chemical knowledge on long-range order in amphiboles (Oberti et al., 2007) provided information on cation ordering and hence on the crystal-chemical formula. In particular, reliable estimates of ^{T}Al (ordered at $T(1)$; Oberti et al., 1995a) could be obtained: they are 0.13(2)and 0.22(2) apfu for samples WIN 4-2 and WIN 9-1, respectively. The first value is quite a bit lower than that provided by EMP (0.29 apfu), which may come from inter-crystalline inhomogeneities. ^{C}Al is significantly disordered between the $M(2)$ and $M(3)$ sites. This latter feature is unusual but coherent with the T of crystallization and bulk-chemistry (Oberti et al., 1995b), and has been observed in other studies involving synthetic ^{C}Mg amphiboles (e.g., Della Ventura et al., 1998a; Hawthorne et al., 2000). When the ^{B}Ca content from EMP analysis is taken as the starting point for the calculation of B cations, SREF results confirm the presence of significant amounts of

321 ^{B}Mg and of an amount of ^{A}Na equal to (or slightly higher than) that of $^{T(1)}$Al. All these features
322 were later confirmed by FTIR analysis.

323 As regards the presence of ordered domains or microinclusions of a $P2_1/m$ ^{B}(NaMg)
324 amphibole, examination of the diffraction patterns collected with the area detector did not show
325 any evidence of reflections not explained by the $C2/m$ space group.

326 **TEM analysis**

327 Three samples (WIN 10-1, WIN 1-1, and WIN 11-4) were examined by TEM. Particular
328 attention was paid to WIN 11-4 because it was synthesized at the lowest temperature (760°C)
329 and was thought to be the most likely to display ordered domains as well as the presence of
330 pyroxene or wide-chain defects. About 25 crystals of WIN 11-4 and 5-6 crystals of the other
331 samples were examined using selected-area and convergent-beam electron diffraction as well as
332 HRTEM imaging for lattice defects. Crystals were generally oriented with [100] or [U0W]
333 parallel to the electron beam to look for primitive lattice reflections, but no primitive reflections
334 of the type $h+k \neq 2n$ could be observed. Some chain multiplicity faults (i.e., non-double chain
335 defects) were observed, but not at levels sufficient to affect the bulk composition of the
336 amphibole (e.g. Bozhilov et al., 2007).

337 **FTIR analysis**

338 Infrared spectra obtained at room temperature for samples that were left at atmospheric
339 conditions generally had broad absorption bands that were centered near 3400 cm^{-1}, as seen in
340 the top spectrum of Figure 6 (sample WIN 4-2). Treatment of this sample at temperatures of
341 250-350°C for 10-15 minutes was sufficient to remove this band as seen in the lower spectrum of
342 Figure 6, indicating that it is caused by absorbed moisture and not, for example, to the presence
343 of additional structural OH (Cámara et al., 2004). Because IR spectra measured *in situ* at high

344 temperatures are broader than those at room temperature, the spectra presented here were
345 obtained by first heating the sample to a temperature (300-350°C) suitable to remove all
346 moisture from the pellet and then collecting the spectra upon cooling to 30-40°C.

347 Figure 7a shows the spectra of selected samples along the tremolite–glaucophane join with
348 the absorbed moisture removed. Each spectrum has a dominant central band that occurs in the
349 range 3660-3670 cm^{-1}, and is assigned to an OH dipole adjacent to a vacant *A* site according to
350 the NN (nearest-neighbor) local configuration OH MgMgMg-$^{A}\square$-SiSi for the *M*(1)*M*(1)*M*(3)-*A*-
351 *T*(1)*T*(1) sites (Della Ventura et al., 2003). Less intense but readily identifiable bands occur at
352 both higher and lower wavenumbers and are assigned to OH next to ^{A}Na and ^{C}Al (see below).
353 Figure 7b shows an enlargement of the central band; its shape and shift are the result of several
354 overlapping components which are produced by the change in chemistry of the amphibole along
355 the join. In samples with high ^{B}Ca and low ^{B}Na contents (e.g., WIN 7-1), the band occurs at
356 3672 cm^{-1}; this is the frequency of tremolite. For samples with high ^{B}Na and low ^{B}Ca contents
357 (e.g., WIN 13-3), the same band is centered at 3662 cm^{-1}, which is the frequency observed in
358 glaucophane (Palin et al., 2003) or synthetic glaucophane (Jenkins and Corona, 2006a). The band
359 shift is thus related to the nature of the B cation. As already discussed in previous papers, the
360 effect of B cations on the O-H stretching frequency is small but resolvable, and can even be used
361 to detect short-range ordering (e.g. Gottschalk et al., 1999, Iezzi et al., 2003, Iezzi et al., 2004a,
362 Hawthorne and Della Ventura, 2007). Tremolite is a completely ordered amphibole (Hawthorne,
363 1997) and its spectrum shows an extremely sharp band at 3675 cm^{-1}; due to its sharpness, a
364 minor component related to cummingtonite can be resolved at 3668 cm^{-1} (e.g., Gottschalk et al.,
365 1999, Della Ventura et al., 2003, Hawthorne and Della Ventura, 2007). As discussed in
366 Gottschalk et al. (1999), however, even the pattern of tremolite actually consists of several

overlapping minor components due to the several possible local arrangements of Ca and Mg at the two *M*(4) sites next to the OH dipole. When these configurations with very close frequencies occur in significant amounts, a severe band broadening results, termed "substitutional broadening" (Strens, 1974). In such a case, the FTIR spectrum has insufficient resolution to provide quantitative information on the relative amounts of local ordering patterns. However, it has sufficient resolution to provide qualitative information on the presence of different next-neighbor B cations (Iezzi et al., 2003; Iezzi et al., 2004b; Hawthorne and Della Ventura, 2007). Sample WIN 7-1 has a composition Tr_{82}-Gl_{06}-Cm_{09}-Kt_{03} (Table 5), and shows a broad peak centered at 3672 cm^{-1}, assigned to the CaCa configurations (Figure 7b); sample WIN 13-3 has a composition Tr_{02}-Gl_{76}-Cm_{05}-Kt_{17} (Table 5) and shows a broad peak centered at 3662 cm^{-1}, which is assigned to the NaNa configuration (Jenkins and Corona, 2006a). Samples WIN 4-2 and WIN 12-2, have intermediate compositions Tr_{56}-Gl_{04}-Cm_{11}-Kt_{29} (Table 3) and Tr_{17}-Gl_{38}-Cm_{09}-Kt_{35} (Table 5), respectively, and show a band which can be considered the convolution of three main components, the CaCa, NaNa configurations and a third MgMg configuration at 3668 cm^{-1} attributed to the cummingtonite component. As a general observation, all the spectra are in agreement with the presence of MgMg configurations in solid solution, as shown by asymmetries evident in the spectra. From these observations we can conclude that, in a qualitative way, FTIR spectroscopy shows beyond any doubt the presence of variable local arrangements involving pairs of Ca, Na, and Mg cations in all amphiboles synthesized along the Tr-Gl join. However, the MgMg configuration is restricted to short-range order, because it does not produce any measureable diffraction signal of ordered $P2_1/m$ domains. Mixed configurations, such as NaMg or NaCa etc. are also expected to occur, but these contribute to band broadening and cannot be resolved in these spectra.

At higher wavenumbers, a band appears at about 3720 cm^{-1} starting with sample WIN 7-1, i.e. at Gl_{06}. This band becomes more intense in the series and reaches a maximum intensity for samples WIN 1-1 through WIN 2-2, corresponding to $Gl_{17\text{-}43}$ and $Kt_{36\text{-}39}$. Based on earlier studies on synthetic pargasitic amphiboles (Della Ventura et al., 1999; Della Ventura et al., 2003; Jenkins et al., 2003) and Al-bearing tremolite/richterite (Hawthorne at al., 1996, Della Ventura et al., 1998b), this band can be assigned to the local configuration MgMgMg-^{A}Na-SiAl, i.e. to the presence of partly filled *A* sites in the structure, locally associated with ^{T}Al (ordered at *T*(1), thus confirming the SREF results). The FTIR spectra are thus in agreement with the EMP data which show these samples to have the highest ^{A}Na and ^{T}Al content (Table 3).

At lower wavenumbers, below the central MgMgMg-$^{A}\square$-SiSi band, there is a band at about 3640 cm^{-1} which is relatively constant in intensity beyond the amphibole with the lowest Gl-content (WIN 7-1). Assignment of this band can be based on the study of aluminous tremolites by Hawthorne et al. (2000), who deduced that this band arises from either the presence of Al at the nearest-neighbor *M*(3) site, giving the configuration MgMgAl-$^{A}\square$-SiSi, or to the presence of Al at one of the *T*(1) sites and Al at an *M*(2) site, both at next-nearest-neighbor sites, giving the configuration MgMgMg-$^{A}\square$-SiAl-MgMgAl. Of these two options, the first assignment seems the more likely because essentially all ^{T}Al is paired with ^{A}Na as discussed above for the band at 3720 cm^{-1} and as shown in Figure 4a; furthermore, there is crystal-chemical evidence for Al at the *M*(3) site based on the relative values of the <*M*(2)-O> and <*M*(3)-O> bond-lengths.

Discussion

Amphiboles formed along the tremolite–glaucophane join show a clear deviation from the expected or nominal compositions, particularly near the middle of this join. Efforts to "pull

back" amphiboles to the compositional join by changing the synthesis conditions were not successful (Table 2), such that increased temperatures caused melting, multiple treatments at a given temperature promoted dissolution or melting, and treatments at lower temperatures led to the formation of talc. In all cases the composition of the amphibole was essentially unaffected (Fig. 3b, shaded squares).

There is some evidence that this type of compositional shift also exists for winchites. Figure 8 is a plot of amphiboles reported in the literature (open symbols) from a variety of geological settings, along with the amphiboles reported here (solid symbols). This figure uses the same type of projection scheme used in Figure 3b, but includes Fe^{3+} with Na and Al and combines Fe^{2+} with Mg. Of the samples plotted in Figure 8, only some of the samples from the hydrothermally-altered biotite pyroxenites of the Rainy Creek Complex, Montana, USA, (Meeker et al., 2003) plot near or on the tremolite–glaucophane join. The majority of the samples show deviations from the ideal join, including those from the type locality of winchite occurring in manganese-rich quartzites and schists from Kajlidongri in the Jhabua District, Madhya Pradesh, India (Leake et al., 1986), from a contact zone of the Ilmen alkaline massif, Ilmen Mountains, Russia (Sokolova et al., 2001), in eclogites from Margarita Island, Venezuela (Maresch et al. 1982), and from the western Tianshan metamorphic belt, China (Su et al., 2009). We note that solid solution of amphibole components other than katophorite, such as magnesio-hornblende (MgHb, Fig. 8), may cause deviation from the ideal join in this projection scheme; unfortunately, it is not simple to discern which solid solution is responsible for chemically complex amphiboles. Rather, this figure is offered to emphasize that deviations from the tremolite–glaucophane join are not uncommon.

435 In general, there are very few reports in the literature of winchite (cf. Sokolova et al., 2001
436 for a review). Nearly all of them have significant deviations from ideal stoichiometry, including
437 the presence of larger cations (Fe or Mn), significant ^{T}Al, and A cations. This observation, along
438 with the inability to synthesize ideal winchite in this study, suggests that its cation arrangement is
439 not particularly stable.

440 A positive deviation from ideal mixing (Fig. 5a) is evident from the volume-composition
441 curve for this join, even after the amphiboles are corrected for the Cm and Kt components (Fig.
442 5b). This is consistent with the occurrence of a miscibility gap as mentioned above. The
443 location of this miscibility gap using experimental, compositional, and spectroscopic methods
444 has been briefly discussed by Jenkins (2011) and Jenkins et al. (2011), and will be described in
445 greater detail in a subsequent manuscript.

446 The results from SREF analysis can be combined with the FTIR spectra to shed light on
447 cation order in these samples. First, the presence of CaCa, MgMg, and NaNa clusters at adjacent
448 *M*(4) sites is shown by distinct bands (3672, 3668, and 3662 cm^{-1}) discernible in the main OH-
449 stretching band going from Tr- to Gl-rich compositions. Second, the local cluster corresponding
450 to MgMgMg-^{A}Na-SiAl that produces the 3720 cm^{-1} band reaches a maximum for samples with a
451 nominal 50-80 mol% Gl component, indicating a preferred association of ^{A}Na with ^{T}Al (ordered
452 at *T*(1)) and thus confirming significant deviation from ideal solid-solution. This local order,
453 which corresponds to the well-known edenite exchange vector in amphibole compositional
454 space, was first identified by Hawthorne et al. (1996) in tremolite having Na, K, and Al as its
455 main impurities, and discussed in the context of bond-valence theory by Hawthorne (1997). The
456 absence, or at least very low intensity, of a band at 3730 cm^{-1} attributed to ^{A}Na associated only
457 with $^{T(1)}$Si as in richterite (Na(CaNa)$Mg_5Si_8O_{22}(OH)_2$; Della Ventura et al., 1999), supports this

458 strong short-range order of Na and Al. Third, the appearance of a band at 3640 cm^{-1} is attributed
459 to the configuration MgMgAl-$^{A}\square$-SiSi where OH is next to a vacant *A* site and Al is present at
460 the nearest-neighbor *M*(3) site. The presence of this configuration, which is associated with the
461 glaucophane substitution of ^{B}Na + ^{C}Al for ^{B}Ca + ^{C}Mg, confirms SREF evidence that disordering
462 of Al occurs over the *M*(2) and *M*(3) sites. Hence, ^{C}Al disorder was first suggested as an oddity
463 due to very peculiar chemical and *T* conditions of crystallization, but it is now becoming a
464 characteristic crystal-chemical feature. Other Mg-rich amphiboles formed at relatively high
465 temperatures also display ^{C}Al disorder, namely pargasitic amphiboles from the Finero complex,
466 Italy (Oberti et al., 1995b), synthetic pargasite (Della Ventura et al., 1998a), and synthetic
467 aluminous tremolite (Hawthorne et al., 2000).

468 This study provides basic information on the synthesis and crystal-chemistry of amphiboles
469 formed from bulk compositions along the tremolite–glaucophane join. High-temperature FTIR
470 measurements were used to remove the strong and interfering signal from absorbed water, from
471 which short-range ordering information in the OH-stretching region can be extracted. The
472 information presented in the iron-free system studied here provides a basic framework for
473 understanding iron-bearing actinolite and glaucophane solid solutions in a variety of rocks,
474 particularly high-pressure eclogites and blueschists, as indicated in Figure 8. A separate study of
475 the miscibility gap and energetics of cation mixing for amphiboles along this same join is
476 forthcoming, in which the compositional variation of calcium, sodium-calcium, and sodium
477 amphiboles in response to variation in conditions of metamorphism will be considered.

478 **Acknowledgments**

Financial support for this project from the NSF grant EAR-0947175 to DMJ and from the MIUR-grant 2009NHLC57_006 to RO is gratefully acknowledged. The authors appreciate the thorough reviews provided by F. C. Hawthorne and M. D. Welch.

References Cited

Abo-Mosallam, H. A., Darwish, H., and Salman, S. M. (2010) Crystallization characteristic and properties of some zinc containing soda lime silicate glasses. Journal of Materials Science: Materials Electronics, 21, 889-896.

Basora, A. M., Jenkins, D. M., and Bish, D. L. (2012) The lower-pressure stability of glaucophane in the presence of paragonite and quartz in the system Na_2O-MgO-Al_2O_3-SiO_2-H_2O. American Mineralogist, 97, 713-726.

Boffa Ballaran, T., Carpenter, M. A., Domeneghetti, M. C., and Tazzoli, V. (1998) Structural mechanisms of solid solution and cation ordering in augite-jadeite pyroxenes: I. A macroscopic perspective. American Mineralogist, 83, 419-433.

Bozhilov, K. N. Brownstein, D., and Jenkins, D. M. (2007) Biopyribole evolution during tremolite synthesis from dolomite and quartz in CO_2-H_2O fluid. American Mineralogist, 92, 898-908.

Brown, I.D. and Shannon, R.B. (1973) Empirical bond-strength-bond lengths curves for oxides. Acta Crystallographica, A29, 266-282.

Bruker (2003) SAINT Software Reference Manual. Version 6. Bruker AXS Inc., Madison, Wisconsin, USA.

Cámara, F., Oberti, R., Iezzi, G., Della Ventura, G. (2003) The $P2_1/m \rightarrow C2/m$ phase transition in the synthetic amphibole Na (NaMg) Mg_5 Si_8 O_{22} $(OH)_2$: Thermodynamic and crystal-chemical evaluation. Physics and Chemistry of Minerals, 30, 570-581.

Cámara, F., Oberti, F., Della Ventura, G., Welch, M.D., and Maresch, W.V. (2004) The crystal-structure of synthetic $NaNa_2Mg_5Si_8O_{21}(OH)_3$, a triclinic $C\bar{1}$ amphibole with a triple-cell and excess hydrogen. American Mineralogist, 89, 1464-1473.

Carman, J.H. and Gilbert, M.C. (1983) Experimental studies of glaucophane stability. American Journal of Science, 283-A, 414-437.

Carpenter, M. A. (1979) Omphacites from Greece, Turkey, and Guatemala: composition limits of cation ordering. American Mineralogist, 64, 102-108.

Carpenter, M. A. (1981) Time-temperature-transformation (TTT) analysis of cation disordering in omphacite. Contributions to Mineralogy and Petrology, 78, 433-440.

Cho, M. and Ernst, W. G. (1991) An experimental determination of calcic amphibole solid solution along the join tremolite-tschermakite. American Mineralogist, 76, 985-1001.

Corona, J. C. and Jenkins, D. M. (2007) An experimental investigation of the reaction: glaucophane + 2 quartz = 2 albite + talc. European Journal of Mineralogy, 19, 147-158.

Della Ventura, G., Robert, J. L., Hawthorne, F. C., Raudsepp, M., and Welch, M. D. (1998a) Contrasting patterns of $^{[6]}$Al order in synthetic pargasite and Co-substituted pargasite. Canadian Mineralogist, 36, 1237-1244.

Della Ventura, G., Robert, J.L., Hawthorne, F.C. (1998b) Characterization of short-range order in potassium-fluor-richterite by infrared spectroscopy in the OH-stretching region. Canadian Mineralogist, 36, 181-186.

Della Ventura, G., Hawthorne, F.C., Robert, J.L., Delbove, F., Welch, M., Raudsepp, M. (1999)

Short-range order of cations in synthetic amphiboles along the richterite-pargasite join. European Journal of Mineralogy, 11, 79-94.

Della Ventura, G., Hawthorne, F.C., Robert, J.-L., Iezzi, G. (2003) Synthesis and infrared spectroscopy of amphiboles along the tremolite – pargasite join. European Journal of Mineralogy, 15, 341-347.

Della Ventura, G., Iezzi, G., Redhammer, G. J., Hawthorne, F. C., Scaillet, B., and Novembre, D. (2005) Synthesis and crystal-chemistry of alkali amphiboles in the system Na_2O-MgO-FeO-Fe_2O_3-SiO_2-H_2O as a function of f_{O2}. American Mineralogist, 90, 1375-1383.

Ernst, W.G. (1961) Stability regions of glaucophane. American Journal of Science, 259, 735-765.

Ernst, W.G. (1963) Polymorphism in alkali amphiboles. American Mineralogist, 48, 241-260.

Ghose, S., Kersten, M., Langer, K., Rossi, G., Ungaretti, L. (1986) Crystal field spectra and Jahn Teller effect of Mn^{3+} in clinopyroxene and clinoamphiboles from India. Physics and Chemistry of Minerals, 13, 291-305.

Gottschalk, M., Andrut, M., and Melzer, S. (1999) The determination of the cummingtonite content of synthetic tremolite. European Journal of Mineralogy, 11, 967-982.

Graham, C. M., Maresch, W. V., Welch, M. D., and Pawley, A. R. (1989) Experimental studies on amphiboles: a review with thermodynamic perspectives. European Journal of Mineralogy, 1, 535-555.

Green, E., Holland, T., and Powell, R. (2007) An order-disorder model for omphacitic pyroxene in the system jadeite-diopside-hedenbergite-acmite, with applications to eclogitic rocks. American Mineralogist, 92, 1181-1189.

Hawthorne, F. C. (1997) Short-range order in amphiboles: A bond-valence approach. Canadian Mineralogist, 35, 203-218.

Hawthorne, F. C. and Della Ventura, G. (2007) Short-range order in amphiboles. In, F.C. Hawthorne, R. Oberti, G. Della Ventura, and A. Mottana (eds.) Amphiboles: crystal chemistry, occurrence, and health issues. Reviews in Mineralogy and Geochemistry, 67, 173-222.

Hawthorne, F.C. and Grundy, H. D. (1976) The crystal chemistry of the amphiboles: IV. X-ray and neutron refinements of the crystal structure of tremolite. Canadian Mineralogist, 14, 334-345.

Hawthorne, F. C., and Oberti, R. (2007) Amphiboles: Crystal chemistry. In, F.C. Hawthorne, R. Oberti, G. Della Ventura, and A. Mottana (eds.) Amphiboles: crystal chemistry, occurrence, and health issues. Reviews in Mineralogy and Geochemistry, 67, 1-54.

Hawthorne, F. C., Della Ventura, G., and Robert, J.-L. (1996) Short-range order of (Na,K) and Al in tremolite: An infrared study. American Mineralogist, 81, 782-784.

Hawthorne, F. C., Della Ventura, G., Robert, J.-L., Welch, M. D., Raudsepp, M., and Jenkins, D. M. (1997) A Rietveld and infrared study of synthetic amphiboles along the potassium-richterite-tremolite join. American Mineralogist, 82, 708-716.

Hawthorne, F. C., Welch, M. D., Della Ventura, G., Robert, J. L., and Jenkins, D. M. (2000) Short-range order in synthetic aluminous tremolites: An infrared and triple-quantum MAS NMR study. American Mineralogist, 85, 1716-1724.

Hawthorne, F. C., Oberti, R., and Martin, R. F. (2006) Short-range order in amphiboles from the Bear Lake Diggings, Ontario. Canadian Mineralogist, 44, 1171-1179.

Hawthorne, F.C. and Oberti, R. (Co-Chairs), Harlow, G.E., Maresch, W.V., Martin, R.F., Schumacher, J.C., and, Welch, M.D. (2012) Nomenclature of the amphibole supergroup. American Mineralogist, in press. DOI: http://dx.doi.org/10.2138/am.2012.4276.

Hill, R. J. and Flack, H. D. (1987) The use of the Durbin-Watson *d* statistic in Rietveld analysis. Journal of Applied Crystallography, 20, 356-361.

Himmelberg, G. R. and Papike, J. J. (1969) Coexisting amphiboles from blueschist facies metamorphic rocks. Journal of Petrology, 10, 102-114.

Hirschmann, M., Evans, B. W., and Yang, H. (1994) Composition and temperature dependence of Fe-Mg ordering in cummingtonite-grunerite as determined by X-ray diffraction. American Mineralogist, 79, 862-877.

Holland, T. J. B (1983) The experimental determination of activities in disordered and short-range ordered jadeitic pyroxenes. Contributions to Mineralogy and Petrology, 82, 214-220.

Hovis, G. L., Brennan, S., Keohane, M., and Crelling, J. (1999) High-temperature X-ray investigation of sanidine-analbite crystalline solutions: thermal expansion, phase transitions, and volumes of mixing. Canadian Mineralogist, 37, 701-709.

Hovis, G. L. and Graeme-Barber, A. (1997) Volumes of K-Na mixing for low albite-microcline crystalline solutions at elevated temperature: A test of regular solution thermodynamic models. American Mineralogist, 82, 158-164.

Iezzi, G., Della Ventura, G., Cámara, F., Pedrazzi, G. e Robert, J.-L. (2003) BNa-BLi solid-solution in A-site vacant amphiboles: synthesis and cation ordering along the ferri-clinoferroholmquistite - riebeckite join. American Mineralogist, 88, 955-961.

Iezzi, G., Cámara, F., Della Ventura, G., Oberti, R., Pedrazzi, G. e Robert, J.-L. (2004a) Synthesis, crystal structure and crystal-chemistry of ferri-clinoholmquistite,

□$Li_2Mg_3Fe^{3+}{}_2Si_8O_{22}(OH)_2$. Physics and Chemistry of Minerals, 31, 375-385.

Iezzi, G., Della Ventura, G., Oberti, R., Cámara, F., Holtz, F. (2004b) Synthesis and crystal-chemistry of the synthetic $P2_1/m$ amphibole $Na(NaMg)Mg_5Si_8O_{22}(OH)_2$. American Mineralogist, 89, 640-646.

Jenkins, D. M. (2011) The transition from blueschist to greenschist facies modeled by the reaction glaucophane + 2 diopside + 2 quartz = tremolite + 2 albite. Contributions to Mineralogy and Petrology, 162, 725-738.

Jenkins, D. M. and Corona, J. C. (2006a) The role of water in the synthesis of glaucophane. American Mineralogist, 91, 1055-1068.

Jenkins, D. M. and Corona, J. C. (2006b) Molar volume and thermal expansion of glaucophane. Physics and Chemistry of Minerals, 33, 356-362.

Jenkins, D. M., Bozhilov, K. N., Ishida, K. (2003) Infrared and TEM characterization of amphiboles synthesized near the tremolite-pargasite join in the ternary system tremolite-pargasite-cummingtonite. American Mineralogist, 88, 1104-1114.

Jenkins, D. M., Carpenter, M. A., and Zhang, M. (2011) Asymmetry of the tremolite-glaucophane miscibility gap defined by IR spectra. Geological Society of America, Abstracts with Programs, 43(5), 92, Abstract 29-7.

Koons, P.O. (1982) An experimental investigation of the behavior of amphibole in the system Na_2O-MgO-Al_2O_3-SiO_2-H_2O at high pressures. Contributions to Mineralogy and Petrology, 79, 258-267.

Larson, A. C. and Von Dreele, R. B. (2000) General Structure Analysis System (GSAS). Los Alamos National Laboratory Report LAUR 86-748.

612 Leake, B. E., Farrow, C. M., Chao, F., and Nayak, V. K. (1986) Winchite re-discovered from the
613 type locality in India. Mineralogical Magazine, 50, 173-175.
614 Leake, B. W., Woolley, A. R., Arps, C. E. S., Birch, W. D., Gilbert, M. C., Grice, J. D.,
615 Hawthorne, F. C., Kato, A., Kisch, H. J., Krivovichev, V. G., Linthout, K., Laird, J.,
616 Mandarino, J. A., Maresch, W. V., Nickel, E. H., Rock, N. M. S., Schumacher, J. C., Smith,
617 D. C., Stephenson, N. C. N., Ungaretti, L., Whittaker, E. J. W., and Youzhi, G. (1997)
618 Nomenclature of amphiboles: Report of the subcommittee on amphiboles of the
619 International Mineralogical Association, commission on new minerals and mineral names.
620 American Mineralogist, 82, 1019-1037.
621 Levien, L. and Prewitt, C. T. (1981) High-pressure structural study of diopside. American
622 Mineralogist, 66, 315-323.
623 Levien, L., Prewitt, C. T., and Weidner, D. J. (1980) Structure and elastic properties of quartz at
624 pressure. American Mineralogist, 65, 920-930.
625 Lledo, H. L. and Jenkins, D. M. (2008) Experimental investigation of the upper thermal stability
626 of Mg-rich actinolite; implications for Kiruna-type iron deposits. Journal of Petrology, 49,
627 225-238.
628 Maresch, W.V. (1977) Experimental studies on glaucophane: an analysis of present knowledge.
629 Tectonophysics, 43, 109-125.
630 Maresch, W. V., Medenbach, O., and Rudolph, A. (1982) Winchite and the actinolite-
631 glaucophane miscibility gap. Nature, 296, 731-732.
632 Meeker, G. P., Bern, A. M., Brownfield, I. K., Lowers, H. A., Sutley, S. J., Hoefen, T. M., and
633 Vance, J. S. (2003) The composition and morphology of amphiboles from the Rainy Creek
634 Complex, near Libby, Montana. American Mineralogist, 88, 1955-1969.

635 Müller, W. F. and Compagnoni, R. (2009) Eclogite from the ultrahigh-pressure metamorphic
636 unit at Lago di Cignana, Western Alps: A process-oriented transmission electron microscope
637 study. Lithos, 109, 323-332.
638 Nakamura, D. and Banno, S. (1997) Thermodynamic modelling of sodic pyroxene solid-solution
639 and its application to a garnet-omphacite-kyanite-coesite geothermobarometer for UHP
640 metamorphic rocks. Contributions to Mineralogy and Petrology, 130, 93-102.
641 Nestola, F., Gatta, G. D., and Boffa Ballaran, T. (2006) The effect of Ca substitution on the
642 elastic and structural behavior of orthoenstatite. American Mineralogist, 91, 809-815.
643 Oberti, R., Ungaretti, L., Cannillo, E., Hawthorne, F.C., and Memmi, I. (1995a) Temperature-
644 dependent Al order-disorder in the tetrahedral double-chain of *C*2/*m* amphiboles. European
645 Journal of Mineralogy, 7, 1049-1063.
646 Oberti, R., Hawthorne, F. C., Ungaretti, L., and Cannillo, E. (1995b) $^{[6]}$Al disorder in amphiboles
647 from mantle peridotites. Canadian Mineralogist, 33, 867-878.
648 Oberti, R., Hawthorne, F.C., Cannillo, E., and Cámara, F. (2007) Long-range order in amphiboles.
649 In, F. C. Hawthorne, R. Oberti, G. Della Ventura, A. Mottana, eds., Amphiboles: Crystal
650 Chemistry, Occurrence, and Health Issues, Reviews in Mineralogy and Geochemistry, 67,
651 125-172.
652 Palin, E.J., Guiton, B.S., Craig, M.S., Welch, M.D., Dove, M.T., and Redfern, S.A.T. (2003)
653 Computer simulation of Al-Mg ordering in glaucophane and a comparison with infrared
654 spectroscopy. European Journal of Mineralogy, 15, 893-901.
655 Papike, J. J. and Clark, J. R. (1968) The crystal structure and cation distribution of glaucophane.
656 American Mineralogist, 53, 1156-1173.
657 Pavese, A., Bocchio, R., and Ivaldi, G. (2000) In situ high temperature single crystal X-ray

diffraction study of a natural omphacite. Mineralogical Magazine, 64, 983-993.

Pawley, A.R. (1992) Experimental study of the compositions and stabilities of synthetic nyböite and nyböite-glaucophane amphiboles. European Journal Mineralogy, 4, 71-192.

Pawley, A. R., Graham, C. M., and Navrotsky, A. (1993) Tremolite-richterite amphiboles: synthesis, compositional and structural characterization, and thermochemistry. American Mineralogist 78, 23-35.

Perdikatsis, B. and Burzlaff, H. (1981) Structurverfeinerung am Talk $Mg_3[(OH)_2Si_4O_{10}]$. Zeitshrift für Kristallographie, 156, 177-186.

Prewitt, C.T. and Burnham, C. W. (1966) The crystal structure of jadeite, $NaAlSi_2O_6$. American Mineralogist, 51, 956-975.

Quirion, D.M. and Jenkins, D.M. (1998) Dehydration and partial melting of tremolitic amphibole coexisting with zoisite, quartz, anorthite, diopside, and water in the system H_2O-CaO-MgO-Al_2O_3-SiO_2. Contributions to Mineralogy and Petrology, 130: 379-389.

Reynard, B. and Ballèvre, M. (1988) Coexisting amphiboles in an eclogite from the Western Alps: new constraints on the miscibility gap between sodic and calcic amphiboles. Journal of Metamorphic Geology, 6, 333-350.

Robinson, K., Gibbs, G.V., Ribbe, P.H. (1971) Quadratic elongation: a quantitative measure of distortion in coordination polyhedra, Science, 172, 567-570

Rowbotham, G. and Farmer, V.C. (1974) The effect of "A" site occupancy on the hydroxyl stretching frequency in clinoamphiboles. Contributions to Mineralogy and Petrology, 38, 147-149.

Schumacher, J. C. (2007) Metamorphic amphiboles: composition and coexistence. In, F. C. Hawthorne, R. Oberti, G. Della Ventura, A. Mottana, eds., Amphiboles: Crystal Chemistry,

Occurrence, and Health Issues, Reviews in Mineralogy and Geochemistry, 67, 359-416.

Sharma, A. and Jenkins, D. M. (1999) Hydrothermal synthesis of amphiboles along the tremolite-pargasite join and in the ternary system tremolite-pargasite-cummingtonite. American Mineralogist, 84, 1304-1318.

Sheldrick, G. M. (1996) SADABS. University of Göttingen, Germany.

Smelik, E. A. and Veblen, D. R. (1992) Exsolution of Ca-amphibole from glaucophane and the miscibility gap between sodic and calcic amphiboles. Contributions to Mineralogy and Petrology, 112, 178-195.

Smelik, E.A., Jenkins, D.M., and Navrotsky, A. (1994) A calorimetric study of synthetic amphiboles along the tremolite-tschermakite join and the heats of formation of magnesiohornblende and tschermakite. American Mineralogist, 79:1110-1122.

Sokolova, E. V., Hawthorne, F. C., Gorbatova, V., McCammon, C., Schneider, J. (2001) Ferrian winchite from the Ilmen Mountains, southern Urals, Russia, and some problems with the current scheme for amphibole nomenclature. Canadian Mineralogist, 39, 171-177.

Strens, R.G.J. (1974) The common chain, ribbon and ring silicates. in "The infrared spectra of Minerals", V.C. Farmer, ed.Mineralogical Society, London, 305-330.

Su, W., Zhang, M., Redfern, S. A. T., Gao, J., and Klemd, R. (2009) OH in zoned amphiboles of eclogite from the western Tianshan, NW-China. International Journal of Earth Science (Geologische Rundschau), 98, 1299-1309.

Thompson, S. P. (2008) Structural signatures of medium-range order in annealed laboratory silicates. Astronomy and Astrophysics, 484, 251–265.

Tropper, P., Manning, C.E., Essene, E.J., and Kao, L.S. (2000) The compositional variation of synthetic sodic amphiboles at high and ultra-high pressures. Contributions to Mineralogy

and Petrology, 139, 146-162.

Welch, M.D., and Graham, C.M. (1992) An experimental investigation of glaucophanic amphiboles in the system Na_2O-MgO-Al_2O_3-SiO_2-SiF_2 (NMASF): Some implications for glaucophane stability in natural and synthetic systems at high temperatures and pressures. Contributions to Mineralogy and Petrology, 111, 248- 259.

Yang, H. and Evans, B. W. (1996) X-ray structural refinements of tremolite at 140 and 295 K: Crystal chemistry and petrologic implications. American Mineralogist, 81, 1117-1125.

713 Table 1. Bulk compositions of mixtures investigated in this study

Sample code prefix	Nominal bulk composition	Components* (mole %)
TREM 23	$\square(Ca_{1.8}Mg_{5.2})Si_8O_{22}(OH)_2$	$Tr_{90}Cm_{10}$
TREM 26	$\square(Ca_{1.9}Mg_{5.1})Si_8O_{22}(OH)_2$	$Tr_{95}Cm_5$
WIN 7	$\square(Na_{0.2}Ca_{1.8})(Mg_{4.8}Al_{0.2})Si_8O_{22}(OH)_2$	$Tr_{90}Gl_{10}$
WIN 8	$\square(Na_{0.4}Ca_{1.6})(Mg_{4.6}Al_{0.4})Si_8O_{22}(OH)_2$	$Tr_{80}Gl_{20}$
WIN 3	$\square(Na_{0.4}Ca_{1.44})(Mg_{4.76}Al_{0.4})Si_8O_{22}(OH)_2$	$Tr_{72}Cm_8Gl_{20}$
WIN 9	$\square(Na_{0.6}Ca_{1.4})(Mg_{4.4}Al_{0.6})Si_8O_{22}(OH)_2$	$Tr_{70}Gl_{30}$
WIN 10	$\square(Na_{0.8}Ca_{1.2})(Mg_{4.2}Al_{0.8})Si_8O_{22}(OH)_2$	$Tr_{60}Gl_{40}$
WIN 4	$\square(Na_{0.8}Ca_{1.08})(Mg_{4.32}Al_{0.8})Si_8O_{22}(OH)_2$	$Tr_{54}Cm_6Gl_{40}$
WIN 1	$\square(Na_{1.0}Ca_{1.0})(Mg_{4.0}Al_{1.0})Si_8O_{22}(OH)_2$	$Tr_{50}Gl_{50}$
WIN 11	$\square(Na_{1.2}Ca_{0.8})(Mg_{3.8}Al_{1.2})Si_8O_{22}(OH)_2$	$Tr_{40}Gl_{60}$
WIN 5	$\square(Na_{1.2}Ca_{0.72})(Mg_{3.88}Al_{1.2})Si_8O_{22}(OH)_2$	$Tr_{36}Cm_4Gl_{60}$
WIN 12	$\square(Na_{1.4}Ca_{0.6})(Mg_{3.6}Al_{1.4})Si_8O_{22}(OH)_2$	$Tr_{30}Gl_{70}$
WIN 2	$\square(Na_{1.6}Ca_{0.4})(Mg_{3.4}Al_{1.6})Si_8O_{22}(OH)_2$	$Tr_{20}Gl_{80}$
WIN 13	$\square(Na_{1.8}Ca_{0.2})(Mg_{3.2}Al_{1.8})Si_8O_{22}(OH)_2$	$Tr_{10}Gl_{90}$
FEGL 5	$\square Na_2Mg_3Al_2Si_8O_{22}(OH)_2$	Tr_0Gl_{100}
AMPH 38	$Na(NaCa)(Mg_4Al)(AlSi_7)O_{22}(OH)_2$	Kt_{100}

714 *Component abbreviations: Cm = $\square Mg_7Si_8O_{22}(OH)_2$; Gl = $\square Na_2(Mg_3Al_2)Si_8O_{22}(OH)_2$; Kt =
715 $Na(NaCa)(Mg_4Al)(AlSi_7)O_{22}(OH)_2$; Ny = $Na(Na_2)(Mg_3Al_2)(AlSi_7)O_{22}(OH)_2$; Tr =
716 $\square Ca_2Mg_5Si_8O_{22}(OH)_2$
717

718 Table 2. Treatment conditions and products of synthesis for mixtures investigated near or on the
719 tremolite–glaucophane join and for katophorite.

Sample Code	Bulk Ca (apfu)	*T* (°C)	*P* (GPa)	t (h)	H_2O (wt%)	Products
TREM 23-13	1.80	801(5)	0.452(5)	458	30.0(2)	Amph, Qtz, Cpx
TREM 26-1	1.90	840(9)	0.630(5)	451	11.8(2)	Amph, Qtz, Cpx, Opx
TREM 26-2*	1.90	840(9)	0.605(5)	527	5.5(10)	Amph, Qtz, trace Cpx
WIN 7-1	1.80	820(10)	1.51(6)	160	4.4(1)	Amph, Cpx, trace Qtz
WIN 8-1	1.60	820(10)	1.53(5)	136	4.3(2)	Amph, trace Cpx
WIN 3-1	1.44	750(5)	2.07(8)	166	3.7(3)	Talc, Cpx, Amph, Qtz
WIN 3-2	1.44	825(10)	1.53(6)	92	3.5(6)	Amph, trace Opx
WIN 3-3	1.44	850(5)	2.05(5)	93	7.2(3)	Opx, Cpx, Amph, Liq
WIN 3-4	1.44	800(5)	2.05(6)	258	6.4(3)	Amph, Talc, Liq
WIN 3-5*	1.44	825(5)	1.83(6)	146	3.6(11)	Amph, Qtz, Liq
WIN 9-1	1.40	820(10)	2.02(5)	304	3.8(7)	Amph, Qtz, trace Cpx
WIN 10-1	1.20	820(10)	2.02(5)	165	4.2(2)	Amph, Qtz
WIN 4-1	1.08	825(5)	2.00(5)	70	3.5(1)	Amph, trace Opx
WIN 4-2	1.08	825(5)	2.02(4)	112	4.3(2)	Amph, Opx
WIN 4-3	1.08	775(10)	2.5(1)	120	5.1(3)	Qtz, Amph, Opx
WIN 4-4	1.08	825(10)	2.4(1)	120	4.6(2)	Amph, Opx
WIN 4-5	1.08	850(5)	2.05(5)	93	3.6(14)	Amph, Opx, Cpx, Liq
WIN 4-6	1.08	800(5)	2.05(6)	258	5.6(2)	Amph, Talc
WIN 4-7*	1.08	825(5)	1.83(6)	146	3.4(10)	Amph, Opx, Liq
WIN 1-1	1.00	800(10)	2.04(6)	292	3.0(10)	Amph, Qtz
WIN 1-2*	1.00	800(5)	1.97(5)	92	3.5(2)	Amph, Qtz, Liq
WIN 11-1	0.80	820(10)	2.02(5)	165	4.3(2)	Amph, Qtz, Liq, trace Opx
WIN 11-2	0.80	800(10)	1.96(6)	311	4.6(1)	Amph, trace Opx, Liq
WIN 11-3	0.80	780(10)	1.97(6)	334	4.2(1)	Amph, Qtz, Liq
WIN 11-4	0.80	760(10)	1.98(5)	166	4.2(1)	Amph, Qtz, trace Talc, Liq

WIN 12-1	0.80	820(10)	2.01(5)	119	4.4(2)	Amph, Qtz, Talc, Cpx
WIN 12-2*	0.60	810(15)	2.01(5)	122	1.8(1)	Amph, Qtz, Liq
WIN 2-2	0.40	790(10)	2.10(5)	117	4.4(2)	Amph, Qtz, Liq, trace Cpx
WIN 13-1	0.20	770(10)	2.51(5)	174	4.8(1)	Amph, Talc, Jad, Qtz
WIN 13-2*	0.20	770(10)	2.50(5)	211	1.5(4)	Amph, Qtz, Jad, Talc
WIN 13-3*	0.20	770(10)	2.50(5)	96	2.0(1)	Amph, Qtz, Jad
FEGL 5-3-4**	0.00	750(10)	2.5(1)	661	3.0(1)	Amph, Qtz, trace Talc, trace Jad
FEGL 5-2-7§	0.00	750(10)	2.5(1)	891	4.4(1)	Amph, Qtz, trace Talc
AMPH 38-1 (Kt) §§	1.0	780(10)	2.02(5)	52	4.2(1)	Amph, Cpx, trace smectite
AMPH 38-1-2*	1.0	750(10)	2.00(5)	236	4.2(1)	Amph, trace Cpx

Uncertainties in last digit shown in parentheses. Abbreviations: Amph = amphibole; Cpx = calcic-clinopyroxene; Liq = quenched liquid, or aqueous solute; Opx = orthopyroxene; Jad = sodic-clinopyroxene; Kt= katophorite; Qtz = quartz

*Retreatment of the previous synthesis attempt.

** This sample was treated four separate times, with intermediate grinding, for the total duration shown to react out intermediate smectite and most of the talc and jadeite.

§This sample was treated seven separate times, with intermediate grinding, for the total duration shown, to react out the intermediate phases jadeite and smectite.

§§Bulk composition is katophorite

730 Table 3. Compositions of amphiboles synthesized in this study, reported as weight% and cations per 23 oxygens of the average of *n*
731 electron microprobe analyses.

Sample	TREM 23-13	TREM 26-2	WIN 7-1	WIN 8-1	WIN 9-1	WIN 10-1	WIN 4-2	WIN 1-1
weight%	(0 mol%, Gl)	(0%)	(10%)	(20%)	(30%)	(40%)	(40%)	(50%)
n	9	10	14	15	15	17	17	14
SiO_2	42.8(17)	59.0(11)	58.9(8)	58.3(11)	58.1(4)	57.7(8)	56.9 (12)	57.0(9)
Al_2O_3	----	0.04(1)	1.0(2)	1.8(2)	3.8(4)	4.8(1)	3.9(5)	6.8(22)
MgO	18.8(9)	25.2(4)	25.0(6)	24.9(4)	23.6(5)	23.4(7)	24.2(8)	22.6(12)
CaO	8.8(7)	12.6(5)	11.5(4)	10.9(4)	9.8(3)	9.0(7)	9.8(5)	7.4(7)
Na_2O	----	0.02(2)	0.8(1)	1.2(2)	2.3(2)	2.9(4)	2.5(2)	3.9(5)
Total	70.5(28)	97.0(14)	97.2(12)	97.0(12)	97.6(7)	97.9(7)	97.4(20)	97.8(9)
cations								
Si	7.99(5)	8.02(4)	7.97(2)	7.91(5)	7.82(4)	7.75(8)	7.71(6)	7.64(14)
^{T}Al	----	0.00	0.03(2)	0.09(5)	0.18(4)	0.25(8)	0.29(6)	0.36(14)
^{C}Al	----	0.00	0.13(4)	0.19(5)	0.42(6)	0.51(10)	0.33(6)	0.72(20)
^{C}Mg	5.00	5.00	4.87(4)	4.81(5)	4.58(6)	4.49(10)	4.67(6)	4.28(20)
^{B}Mg	0.25(13)	0.11(6)	0.18(6)	0.22(4)	0.16(3)	0.20(8)	0.21(8)	0.23(8)
^{B}Ca	1.76(14)	1.84(8)	1.67(6)	1.58(7)	1.42(5)	1.30(11)	1.42(8)	1.07(11)
^{B}Na	----	0.00	0.15(3)	0.20(5)	0.42(6)	0.50(8)	0.37(6)	0.70(11)
^{A}Na	----	0.00	0.06(3)	0.10(5)	0.18(3)	0.24(5)	0.28(5)	0.33(5)
Total	15.01(6)	14.98(4)	15.06(3)	15.10(5)	15.18(3)	15.25(5)	15.30(5)	15.33(5)

732 Note: Uncertainties (1σ) in the last digit based on *n* analyses are given in parentheses. Abbreviations as in Tables 1 and 2.

733 Table 3 – continued

Sample	WIN 11-1	WIN 11-2	WIN11-3	WIN 11-4	WIN 12-2	WIN 2-2	WIN 13-3
weight%	(60%)	(60%)	(60%)	(60%)	(70%)	(80%)	(90%)
n	16	14	15	21	16	16	16
SiO_2	56.6(8)	57.1(17)	56.9(10)	57.5(10)	57.3(6)	57.0(23)	59.8(10)
Al_2O_3	7.4(11)	5.9(6)	7.3(16)	7.8(20)	9.5(10)	10.5(32)	12.0(6)
MgO	22.4(9)	23.3(5)	22.4(8)	21.6(10)	20.3(6)	19.7(21)	17.5(7)
CaO	6.4(6)	7.0(6)	6.1(6)	6.6(6)	4.8(7)	3.3(4)	1.5(4)
Na_2O	4.3(4)	4.1(3)	4.6(4)	4.5(5)	5.6(5)	6.1(11)	7.2(4)
Total	97.1(7)	97.4(16)	97.3(4)	97.9(7)	97.6(6)	96.6(13)	98.0(11)
cations							
Si	7.62(7)	7.68(9)	7.64(13)	7.68(13)	7.65(7)	7.61(25)	7.83(6)
^{T}Al	0.38(7)	0.31(9)	0.35(13)	0.33(13)	0.35(7)	0.39(25)	0.17(6)
^{C}Al	0.80(12)	0.62(8)	0.80(13)	0.90(20)	1.14(12)	1.29(27)	1.69(10)
^{C}Mg	4.20(12)	4.38(8)	4.20(13)	4.09(19)	3.86(12)	3.71(27)	3.31(10)
^{B}Mg	0.29(7)	0.30(8)	0.29(6)	0.19(4)	0.19(3)	0.27(19)	0.10(5)
^{B}Ca	0.93(9)	1.00(9)	0.88(8)	0.94(9)	0.69(10)	0.48(6)	0.22(6)
^{B}Na	0.77(8)	0.69(7)	0.83(6)	0.86(10)	1.12(11)	1.26(16)	1.67(9)
^{A}Na	0.35(4)	0.38(10)	0.38(7)	0.29(5)	0.33(5)	0.35(15)	0.16(6)
Total	15.35(4)	15.38(10)	15.38(7)	15.29(5)	15.33(5)	15.35(15)	15.16(7)

734

735

736 Table 3 - continued

Sample	FEGL 5-3-4	FEGL 5-2-7	WIN 11-1	WIN 11-2	WIN 11-3	WIN 11-4	AMPH 38-1-2
weight%	(100%)	(100%)	(Liq)	(Liq)	(Liq)	(Liq)	(Kt)
n	10	14	5	8	7	11	16
SiO_2	55.8(80)	51.8(88)	68.4(14)	65.3(33)	66.4(24)	63.9(17)	50.7(7)
Al_2O_3	12.1(19)	11.6(19)	11.4(6)	11.5(10)	11.6(6)	10.4(8)	12.1(7)
MgO	14.4(21)	13.3(21)	4.7(23)	4.2(21)	3.9(10)	7.8(23)	20.0(6)
CaO	0.10(2)	0.12(4)	1.8(7)	1.8(8)	1.7(7)	3.0(8)	6.8(4)
Na_2O	6.8(9)	6.7(11)	2.1(7)	4.3(7)	3.6(6)	3.4(4)	7.0(3)
Total	89(13)	83(14)	88(2)	87(1)	87(3)	88(2)	96.6(13)
cations							
Si	7.96(7)	7.91(9)	9.36(24)	9.19(23)	9.29(12)	8.95(20)	6.99(5)
^{T}Al	0.05(5)	0.09(9)	----	----	----	----	1.00(5)
^{C}Al	1.98(5)	1.99(8)	1.85(12)	1.90(12)	1.91(7)	1.72(12)	0.96(8)
^{C}Mg	2.99(4)	2.99(11)	0.96(47)	0.89(46)	0.82(20)	1.62(47)	4.04(8)
^{B}Mg	0.07(5)	0.04(4)	----	----	----	----	0.08(4)
^{B}Ca	0.016(5)	0.02(1)	0.26(10)	0.27(13)	0.25(10)	0.45(12)	1.00(7)
^{B}Na	1.89(5)	1.91(9)	0.56(18)	1.18(21)	0.96(15)	0.92(12)	0.92(6)
^{A}Na	0.01(2)	0.08(9)	----	----	----	----	0.96(4)
Total	14.97(4)	15.04(13)	12.99(39)	13.44(35)	13.23(15)	13.66(25)	15.96(4)

737

738

739 Table 4. Unit-cell dimensions of selected amphiboles listed in Table 2.

Sample Code	Nominal Ca, apfu	*a*, Å	*b*, Å	*c*, Å	β, °	*V*, Å^3	GoF	DW-*d*
TREM 23-13	1.80	9.8033(6)	18.042(1)	5.2736(4)	104.571(6)	902.76(8)	1.80	0.76
TREM 26-2	1.90	9.8148(5)	18.045(1)	5.2746(3)	104.620(5)	903.96(6)	1.71	1.86
WIN 7-1	1.80	9.8164(7)	18.039(2)	5.2757(6)	104.585(8)	904.11(11)	1.82	1.09
WIN 8-1*	1.60	9.8161(4)	18.031(1)	5.2747(3)	104.612(5)	903.39(6)	1.53	1.64
WIN 9-1	1.40	9.7996(4)	17.993(1)	5.2752(3)	104.558(5)	900.29(6)	1.46	1.79
WIN 10-1	1.20	9.7893(4)	17.980(1)	5.2754(3)	104.487(5)	899.00(6)	1.62	1.51
WIN 1-1	1.00	9.7634(4)	17.9304(9)	5.2765(3)	104.380(4)	894.77(6)	1.67	1.54
WIN 11-1	0.80	9.7470(5)	17.920(1)	5.2772(3)	104.268(5)	893.30(6)	1.50	1.58
WIN 12-2	0.60	9.6919(9)	17.857(2)	5.2789(7)	104.056(10)	886.2(1)	1.73	1.31
WIN 2-2	0.40	9.6574(6)	17.800(1)	5.2846(4)	103.942(6)	881.70(7)	1.68	1.35
WIN 13-3	0.20	9.5794(7)	17.715(2)	5.2840(5)	103.766(7)	870.94(9)	1.89	1.42
FEGL 5-3-4	0.00	9.5188(4)	17.6805(9)	5.2896(3)	103.594(4)	865.29(5)	1.78	1.37
FEGL 5-2-7	0.00	9.5211(5)	17.680(1)	5.2895(3)	103.612(5)	865.39(6)	1.99	1.10
AMPH 38-1-2*	1.00	9.8099(6)	17.837(2)	5.2762(5)	104.683(7)	893.06(9)	1.73	1.22

740 Note: Uncertainty in last digit (1σ) is given in parentheses. The whole-pattern refinement indices are: GoF is Goodness of Fit =

741 $R_{wp}/R_{exp} = \sqrt{\chi^2}$; DW-*d* is the Durbin-Watson *d* statistic (Hill and Flack, 1987).

742 *Quartz was not present and therefore could not serve as an internal standard in these samples.

743

744 Table 5. Compositions of selected amphiboles from Table 3 recast into the mole fractions of Tr, Gl, Cm, and Kt or Ny components,
745 and corresponding corrected volumes.

Sample Code	Nominal Ca (apfu)	Amphibole components* (mole fractions)						V_{obs} (Å^3)	V_{corr} (Å^3)
		Tr	Gl	Cm	Kt	Ny	Tr'**		
TREM 23-13	1.80	0.88(7)	0.00	0.12(7)	0.00	----	1.00(10)	902.76(8)	907(3)
TREM 26-2	1.90	0.94(3)	0.00	0.06(3)	0.00	----	1.00(4)	903.96(6)	906(1)
WIN 7-1	1.80	0.82(3)	0.06(2)	0.09(3)	0.03(3)	----	0.93(5)	904.11(11)	907(1)
WIN 8-1*	1.60	0.74(3)	0.05(5)	0.11(2)	0.10(5)	----	0.94(8)	903.39(6)	908(1)
WIN 9-1	1.40	0.62(3)	0.12(4)	0.08(2)	0.18(4)	----	0.84(7)	900.29(6)	905(1)
WIN 10-1	1.20	0.52(9)	0.13(3)	0.10(4)	0.25(8)	----	0.80(18)	899.00(6)	905(4)
WIN 1-1	1.00	0.36(11)	0.17(4)	0.11(4)	0.36(14)	----	0.68(26)	894.77(6)	900(10)
WIN 11-1	0.80	0.28(7)	0.20(7)	0.15(3)	0.37(7)	----	0.58(19)	893.30(6)	899(2)
WIN 12-2	0.60	0.17(6)	0.38(6)	0.09(2)	0.35(7)	----	0.31(12)	886.2(1)	884(1)
WIN 2-2	0.40	0.04(11)	0.43(9)	0.13(9)	0.39(24)	----	0.08(23)	881.70(7)	874(19)
WIN 13-3	0.20	0.02(3)	0.76(6)	0.05(3)	0.17(6)	----	0.02(4)	870.94(9)	866(2)
FEGL 5-3-4	0.00	0.008(3)	0.92(7)	0.03(2)	----	0.04(5)	0.009(3)	865.29(5)	865(1)
FEGL 5-2-7	0.00	0.010(3)	0.88(8)	0.02(2)	----	0.09(8)	0.011(4)	865.39(6)	865(2)

746 Note: V_{corr} is the volume corrected back to the tremolite-glaucophane join using equation 1 in the text. Uncertainty in the last digit
747 (1σ) is given in parentheses.

748 *Amphibole components were calculated from the microprobe analyses in Table 3 as follows. For all but the last two amphiboles the
749 mole fraction of Tr = (^{B}Ca - ^{T}Al)/2, Gl = (^{B}Na - ^{T}Al)/2, Cm = ^{B}Mg/2, and Kt= ^{T}Al. For FEGL 5-3-4 and FEGL 5-2-7 the mole
750 fractions are Tr = ^{B}Ca/2; Gl = [^{B}Na – 2(^{T}Al)]/2; Cm = ^{B}Mg/2; and Ny = ^{T}Al.
751 **Tr' = Tr/(Tr+Gl), which is the mole fraction of Tr excluding Cm, Kt, or Ny components.

752

David M. Jenkins, Giancarlo Della Ventura, Roberta Oberti, Krassimir Bozhilov

Synthesis and characterization of amphiboles along the tremolite–glaucophane join.

Table 6 – Supplementary crystallographic data. Single-crystal refinements (SREF) of samples WIN 9-1 and WIN 4-2

WIN 9-1

a = 9.8076(9) b = 18.0004(17) c = 5.2804(5) Å beta = 104.575(2)° V = 902.21 Å^3

Atom coordinates, refined site-scattering values (ss, epfu), atomic-displacement parameters (B_{eq}, Å^2; β_{ij})

Site	ss	x/a	y/b	z/c	B_{eq}	β_{11}	β_{22}	β_{33}	β_{12}	β_{13}	β_{23}
O(1)	32.00	0.11079	0.08660	0.21658	0.88	0.0020	0.0008	0.0080	-0.00012	0.0010	-0.0001
O(2)	32.00	0.11901	0.17091	0.72730	0.97	0.0029	0.0009	0.0079	0.00019	0.0020	0.0002
O(3)	16.00	0.10967	0.00000	0.71368	1.12	0.0027	0.0009	0.0117	0.00000	0.0012	0.0000
O(4)	32.00	0.36549	0.24850	0.79236	1.24	0.0042	0.0009	0.0103	-0.00020	0.0023	-0.0001
O(5)	32.00	0.34739	0.13453	0.09805	1.15	0.0029	0.0011	0.0092	0.00001	0.0012	0.0008
O(6)	32.00	0.34379	0.11802	0.58993	1.05	0.0030	0.0009	0.0086	0.00016	0.0015	-0.0007
O(7)	16.00	0.33697	0.00000	0.28829	1.14	0.0036	0.0004	0.0145	0.00000	0.0011	0.0000
T(1)	55.80	0.28068	0.08468	0.29671	0.71	0.0020	0.0006	0.0064	-0.00002	0.0013	-0.0001
T(2)	56.00	0.28869	0.17169	0.80393	0.82	0.0024	0.0007	0.0070	-0.00016	0.0011	-0.0000
M(1)	24.00	0.00000	0.08826	0.50000	0.78	0.0024	0.0006	0.0066	0.00000	0.0013	0.0000
M(2)	24.06	0.00000	0.17748	0.00000	0.84	0.0024	0.0008	0.0072	0.00000	0.0018	0.0000
M(3)	24.00	0.00000	0.00000	0.00000	0.83	0.0028	0.0005	0.0081	0.00000	0.0014	0.0000
M(4)	34.56	0.00000	0.27719	0.50000	1.08	0.0035	0.0009	0.0101	0.00000	0.0036	0.0000
A2	2.38	0.00000	0.47927	0.00000	3.20						
H	2.00	0.20284	0.00000	0.76357	1.89						

$\mathbf{R}_{3\sigma}$ = 3.51 (806 refl.) $R_{5\sigma}$ = 2.69 (614 refl.) R_{all} = 7.20 (1369 refl.) F(000)= 805.58 limited to θ = 30°

Selected interatomic distances (Å) and angles (°). Values of tetrahedral (T) and octahedral (O) quadratic elongation (QE) and angular variance (AV) are calculated according to Robinson et al. (1971). DELTA is calculated according to Brown and Shannon (1973)

T(1)-O(1)	1.613	T(2)-O(2)	1.611	M(4)-O(2)	2.400	M(1)-O(1)	2.059	M(2)-O(1)	2.131	M(3)-O(1)	2.072
-O(5)	1.637	-O(4)	1.583	-O(4)	2.316	-O(2)	2.076	-O(2)	2.073	-O(3)	2.064
-O(6)	1.630	-O(5)	1.656	-O(5)	2.770	-O(3)	2.084	-O(4)	1.997	H-O(3)	0.885
-O(7)	1.626	-O(6)	1.676	-O(6)	2.549	<M(1)-O>	2.073	<M(2)-O>	2.067	<M(3)-O>	2.069
<T(1)-O>		<T(2)-O>		<M(4)-O>		VOL.	11.685	VOL.	11.642	VOL.	11.557
1.626		1.631		2.508							

VOL.	2.205	VOL.	2.212		OQE	1.0112	OQE	1.0082	OQE	1.0148
TQE	1.0010	TQE	1.0053		OAV	36.83	OAV	25.61	OAV	48.23
TAV	4.13	TAV	21.70		DELTA	0.254	DELTA	6.963	DELTA	0.031

A -O(5)	2.958	*A*(2)-O(5)	2.664	*T*(1)-*T*(2)-*T*(1)	118.58
-O(6)	3.143	-O(6)	2.904	*T*(1)-O(5)-*T*(2)	136.25
-O(7)	2.469	-O(7)	2.498	*T*(1)-O(6)-*T*(2)	137.95
<*A* -O>	2.934	<*A*(2)-O>	2.688	*T*(1)-O(7)-*T*(1)	139.34
				M(1)-*M*(2)	3.090

WIN 4-2

a = 9.7739(11) *b* = 17.9636(20) *c* = 5.2659(6) Å beta = 104.423(3)° *V* = 895.42 Å^3

Atom coordinates, refined site-scattering values (ss, epfu), atomic-displacement parameters (B_{eq}, Å^2; β_{ii})

Site	ss	x/*a*	y/*b*	z/*c*	B_{eq}	β_{11}	β_{22}	β_{33}	β_{12}	β_{13}	β_{23}
O(1)	32.00	0.11062	0.08673	0.21645	0.65	0.0021	0.0007	0.0034	-0.0001	0.0008	0.0001
O(2)	32.00	0.11904	0.17120	0.72635	0.72	0.0019	0.0006	0.0063	0.0002	0.0009	0.0001
O(3)	16.00	0.10974	0.00000	0.71485	0.76	0.0021	0.0007	0.0059	0.0000	0.0014	0.0000
O(4)	32.00	0.36571	0.24868	0.79115	0.94	0.0037	0.0005	0.0088	-0.0004	0.0023	-0.0001
O(5)	32.00	0.34784	0.13441	0.09800	0.94	0.0032	0.0009	0.0057	0.0001	0.0015	0.0010
O(6)	32.00	0.34347	0.11794	0.58877	0.86	0.0027	0.0010	0.0034	0.0001	0.0009	-0.0010
O(7)	16.00	0.33775	0.00000	0.28706	0.96	0.0029	0.0005	0.0129	0.0000	0.0024	0.0000
T(1)	56.00	0.28063	0.08459	0.29511	0.46	0.0018	0.0004	0.0029	0.0000	0.0009	-0.0001
T(2)	55.80	0.28941	0.17146	0.80351	0.49	0.0020	0.0004	0.0025	-0.0001	0.0008	0.0001
M(1)	24.00	0.00000	0.08830	0.50000	0.57	0.0026	0.0004	0.0024	0.0000	0.0012	0.0000
M(2)	24.33	0.00000	0.17747	0.00000	0.65	0.0022	0.0005	0.0053	0.0000	0.0011	0.0000
M(3)	12.31	0.00000	0.00000	0.00000	0.63	0.0027	0.0003	0.0046	0.0000	0.0009	0.0000
M(4)	34.26	0.00000	0.27693	0.50000	0.95	0.0037	0.0008	0.0078	0.0000	0.0040	0.0000
A	2.90	0.00000	0.50000	0.00000	6.17						
H	2.00	0.19245	0.00000	0.74231	1.31						

$R_{3\sigma}$ = 4.38 (1020 refl.) $R_{5\sigma}$ = 3.82 (863 refl.) R_{all} = 6.34 (1837 refl.) *F*(000)= 805.58 limited to θ = 35°

Selected interatomic distances (Å) and angles (°). Values of tetrahedral (T) and octahedral (O) quadratic elongation (QE) and angular variance (AV) are calculated according to Robinson et al. (1971). DELTA is calculated according to Brown and Shannon (1973)

T(1)-O(1)	1.610	*T*(2)- (O2)	1.613	*M*(4)- (O2)	2.386	*M*(1)-O(1)	2.050	*M*(2)-O(1)	2.124	*M*(3)-O(1)	2.069

-O(5)	1.628	-O(4)	1.584	-O(4)	2.299	-O(2)	2.074	-O(2)	2.068	-O(3)	2.051
-O(6)	1.629	-O(5)	1.653	-O(5)	2.768	-O(3)	2.084	-O(4)	1.993	H-O(3)	0.785
-O(7)	1.623	-O(6)	1.667	-O(6)	2.546	<*M*(1)-O>	2.069	<*M*(2)-O>	2.062	<*M*(3)-O>	2.063
<*T*(1)-O>	1.622	<*T*(2)-O>	1.629	<*M*(4)-O>	2.500	VOL.	11.618	VOL.	11.559	VOL.	11.452
VOL.	2.188	VOL.	2.205			OQE	1.0113	OQE	1.0081	OQE	1.0150
TQE	1.0011	TQE	1.0047			OAV	37.17	OAV	25.22	OAV	48.71
TAV	4.69	TAV	18.79			DELTA	0.462	DELTA	6.748	DELTA	0.169

A -O(5)	2.948	*A*(2)-O(5)	3.005	*T*(1)-*T*(2)-*T*(1)	118.62
-O(6)	3.141	-O(6)	3.619	*T*(1)-O(5)-*T*(2)	136.02
-O(7)	2.448	-O(7)	5.476	*T*(1)-O(6)-*T*(2)	138.38
<*A* -O>	2.925	<*A*(2-O>	4.034	*T*(1)-O(7)-*T*(1)	138.86
				M(1)-*M*(2)	3.082

Figure Captions

Figure 1. Back-scattered electron image of representative samples of the amphiboles formed in this study. (a) Sample TREM 26-2 (nominal $Tr_{95}Cm_{05}$). Lath-shaped crystals are tremolite, with minor lighter-grey grains of clinopyroxene. Scale is 20 μm. (b) Sample WIN 9-1 (nominal $Tr_{70}Gl_{30}$). Large amphibole grain is present in the center of the image. Darker grey interstitial areas are quartz. Scale is 20 μm. (C) Sample WIN 11-1 (nominal $Tr_{40}Gl_{60}$). The prismatic crystals of amphibole are abundant and lighter grey, while the darker interstitial areas are either quartz or silica-rich quenched liquid (or precipitated solute). Scale is 20 μm. (d) Sample FEGL 5-3-4 (nominal Tr_0Gl_{100}). This sample consists of numerous fine needles of glaucophanic amphibole. Scale is 10 μm.

Figure 2. (a) Powder XRD pattern obtained for nominal $Tr_{50}Gl_{50}$ (WIN 1-1) made at 800°C, 2 GPa, 292 hours, with 3 wt% H_2O. The pattern is dominantly amphibole with quartz (Qtz) as a coexisting phase. (b) The same material treated a second time (WIN 1-2) at the same conditions for an additional 92 h. Notice the reduced intensity of the quartz peak and the appearance of a broad amorphous X-ray maximum (liq) centered at about 17.5 °2θ. Vertical dashed lines indicate the location of the quartz peaks in the two patterns.

Figure 3. (a) Compositions of amphiboles (circles) made in this study projected from H_2O onto the $(Na_{0.5}O + AlO_{1.5})$-CaO-MgO-SiO_2 quadrilateral diagram. Shown for reference is the tetrahedral space defined by the ideal components tremolite (Tr), glaucophane (Gl), cummingtonite (Cm), and katophorite (Kt) which completely encompasses the amphibole compositions made in this study. (b) The same amphibole compositions (circles) as shown in (a) but projected from cummingtonite's bulk composition ($Mg_7Si_8O_{22}(OH)_2$) and H_2O onto the $(Na_{0.5}O + AlO_{1.5})$-CaO-SiO_2 ternary plane. The grey symbols are the average

compositions of the amorphous phase (liq, squares), amphiboles (circles), and the bulk composition (triangle) for the WIN 11-1, -2, -3, and -4 synthesis products (Tables 2 and 3). Quartz (Qtz) and the same amphibole end members as shown in (a) are plotted for reference.

Figure 4. Plots showing the strong correlation between Na and Al. (a) ^{A}Na vs ^{T}Al. The diagonal line shows the expected trend for the join tremolite (Tr)–katophorite (Kt). (b) ^{B}Na vs ^{C}Al. The diagonal line shows the expected trend for the join tremolite (Tr)–glaucophane (Gl). Error bars are 1σ uncertainty.

Figure 5. (a) Observed unit-cell volumes in Å^3 of amphiboles formed in this study along the tremolite–glaucophane join plotted as function of the mole fraction of ^{B}Ca. Solid curve is a polynomial fit to the data. (b) Unit-cell volumes after correction for other components (primarily Cm and Kt components; Table 5) and then projected onto the tremolite–glaucophane join. Solid curve is the same polynomial curve as shown in (a). Dashed line represents ideal mixing (mechanical mixture) between the end members.

Figure 6. Top pattern is a representative FTIR spectrum of an intermediate amphibole (WIN 4-2) measured at room temperature and showing a strong curve at about 3400 cm^{-1} from absorbed water. Bottom pattern is the same sample after heating to 350°C for about 15 minutes, removing the absorbed moisture and revealing additional information about cation ordering.

Figure 7. (a) FTIR spectra for selected samples measured at 30-40°C after heating to 250-350°C to remove absorbed moisture. Samples are ordered from bottom to top in the sequence of lowest to highest Gl content, respectively. (b) Enlarged view of the main OH-stretching bands of the spectra in (a). Vertical dashed lines show the positions of three distinct bands at about 3672, 3668, and 3662 cm^{-1} changing in intensities with increasing Gl content.

Figure 8. Compositions of amphiboles reported in the literature (open symbols) from a variety of geological settings plotted along with the amphiboles reported here (solid symbols). Compositions are plotted using a projection scheme similar to that in Figure 3b but combining Fe^{3+} with Na^{+} and Al^{3+} and combining Fe^{2+} with Mg^{2+}. This plot illustrates that, although some amphiboles come close to the ideal tremolite–glaucophane join, there are many that deviate in a manner similar to what is observed here. Magnesio-hornblende ($\square Ca_2(Mg_4Al)(AlSi_7)O_{22}(OH)_2$) plots at the point labeled MgHb; other abbreviations as in Figure 3b.

878 Figure 1

879

880 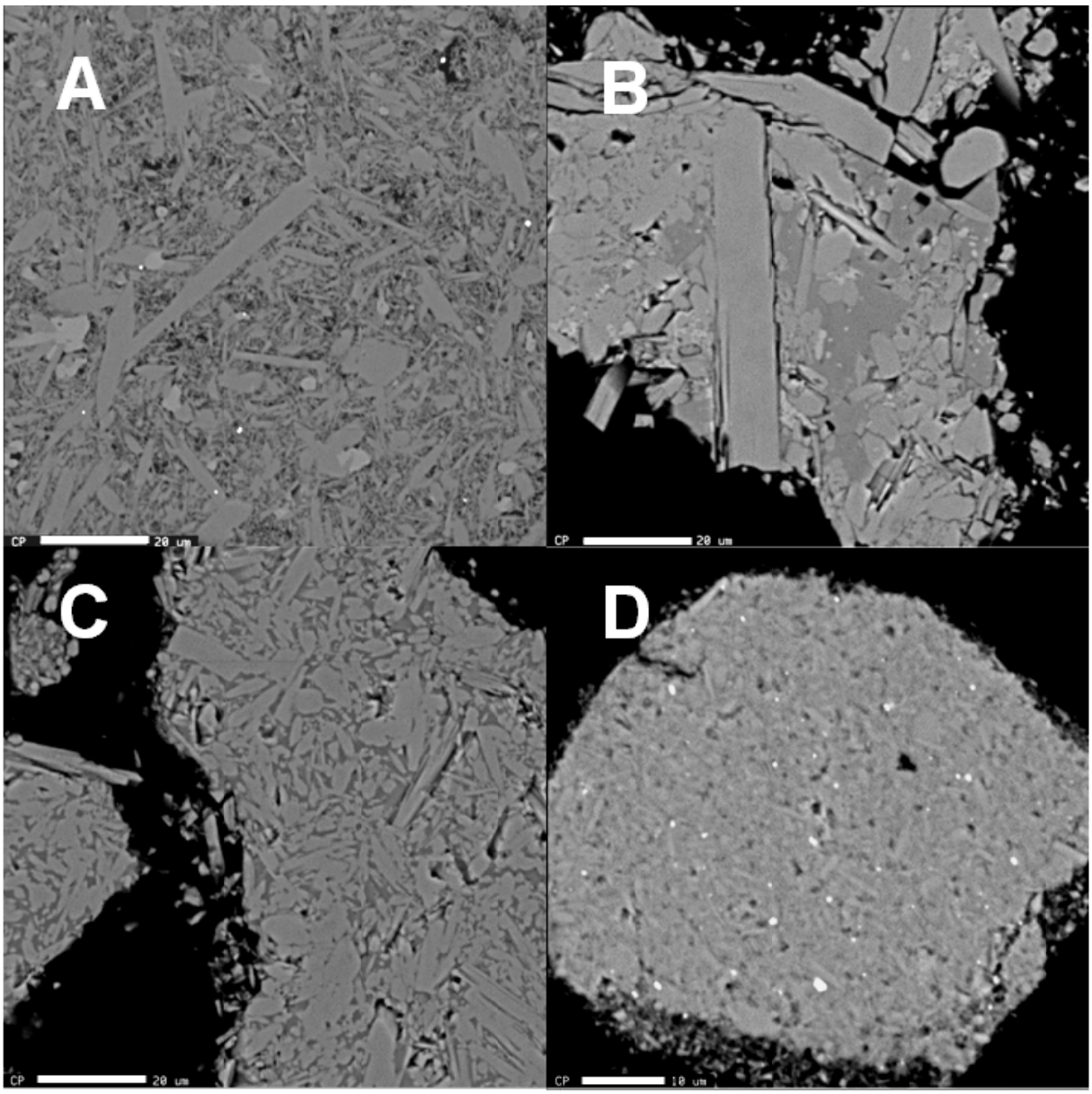

881 Figure 2

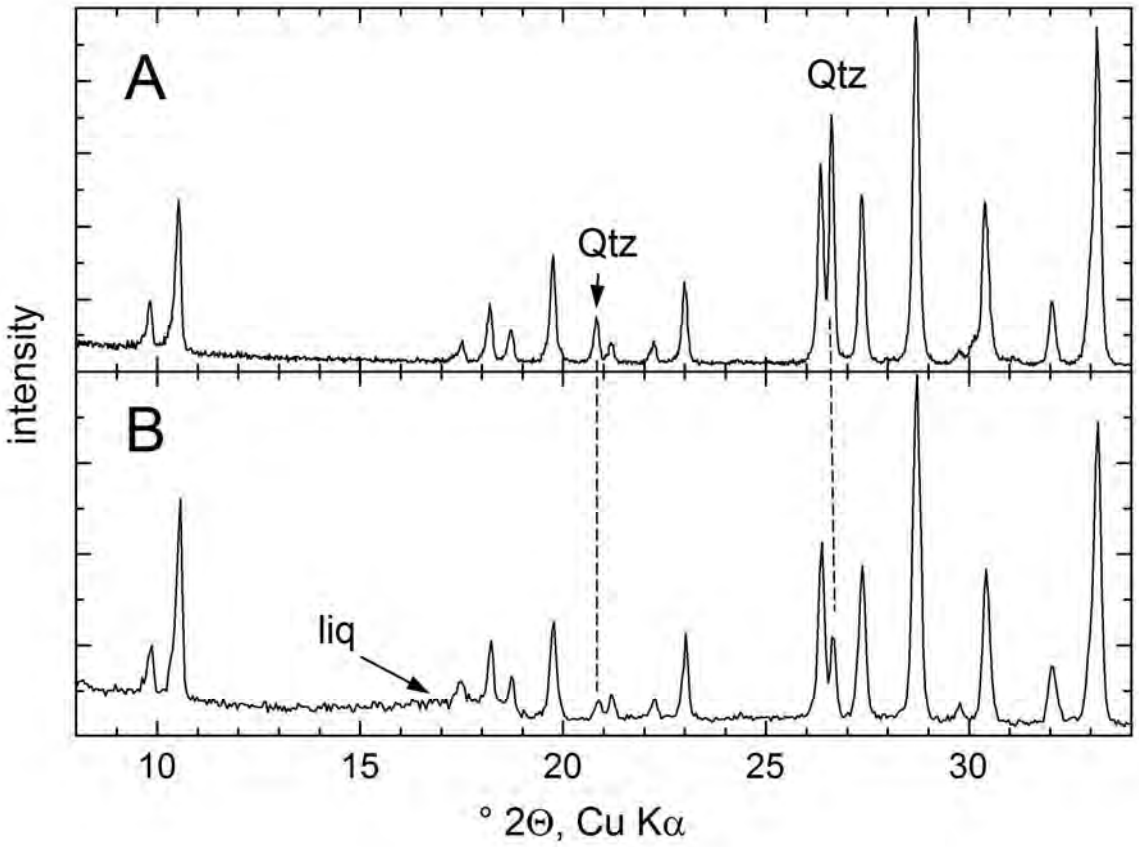

882

883

884 Figure 3

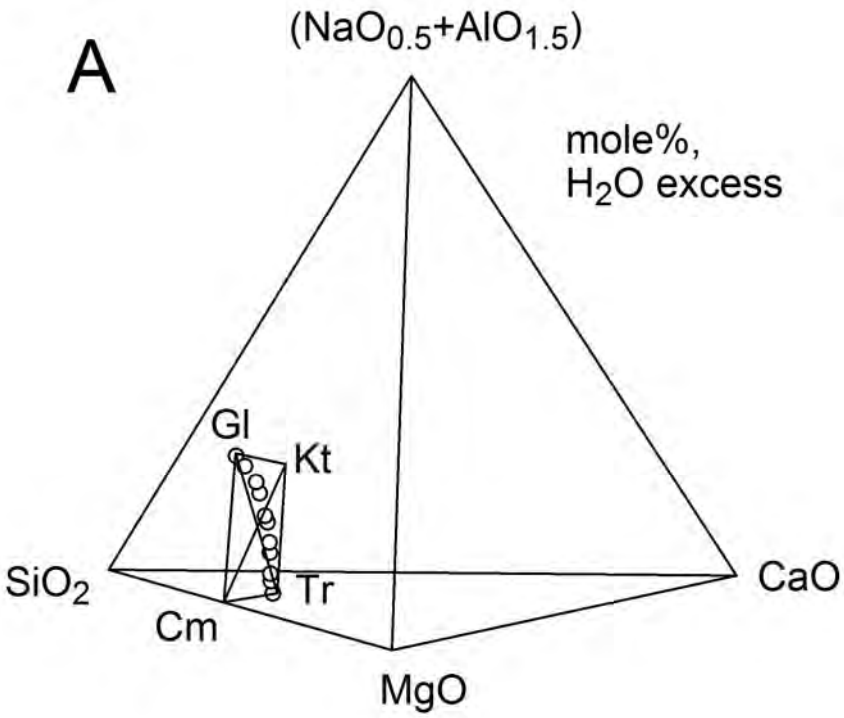

885

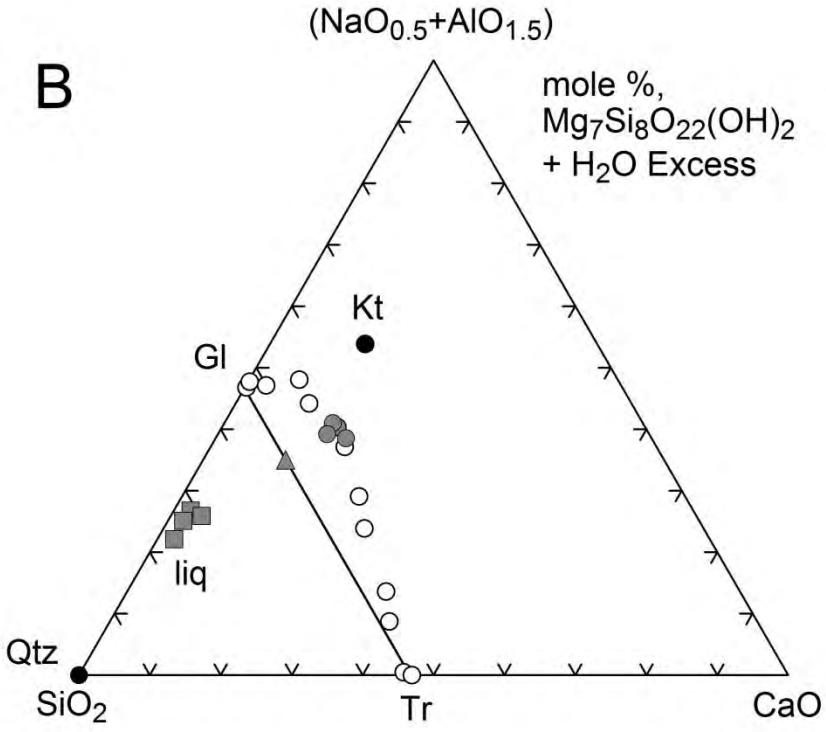

886

887

888 Figure 4.

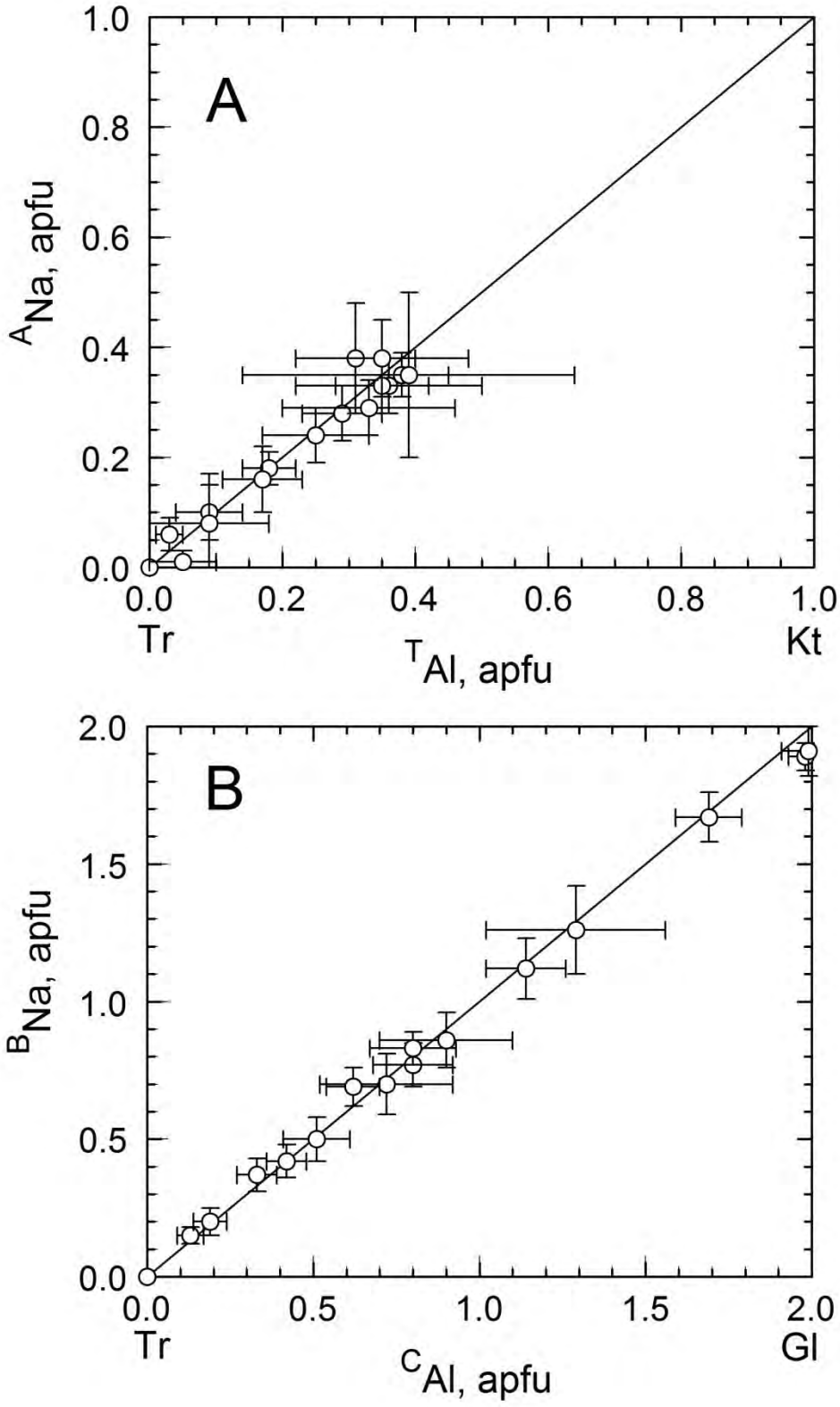

889

890 Figure 5

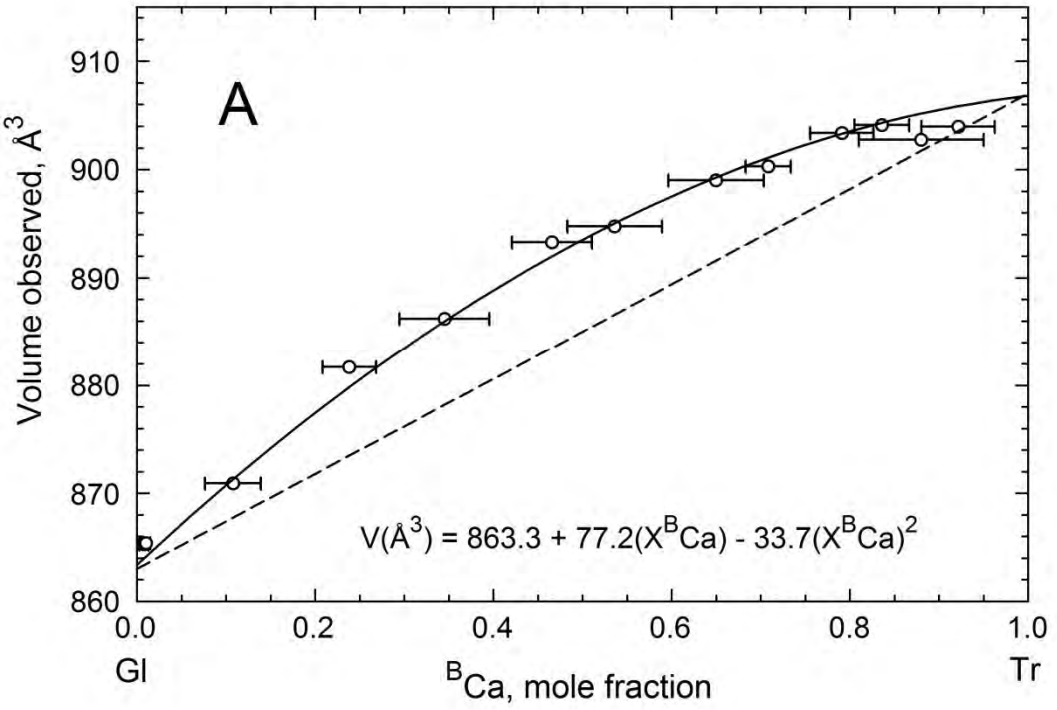

891

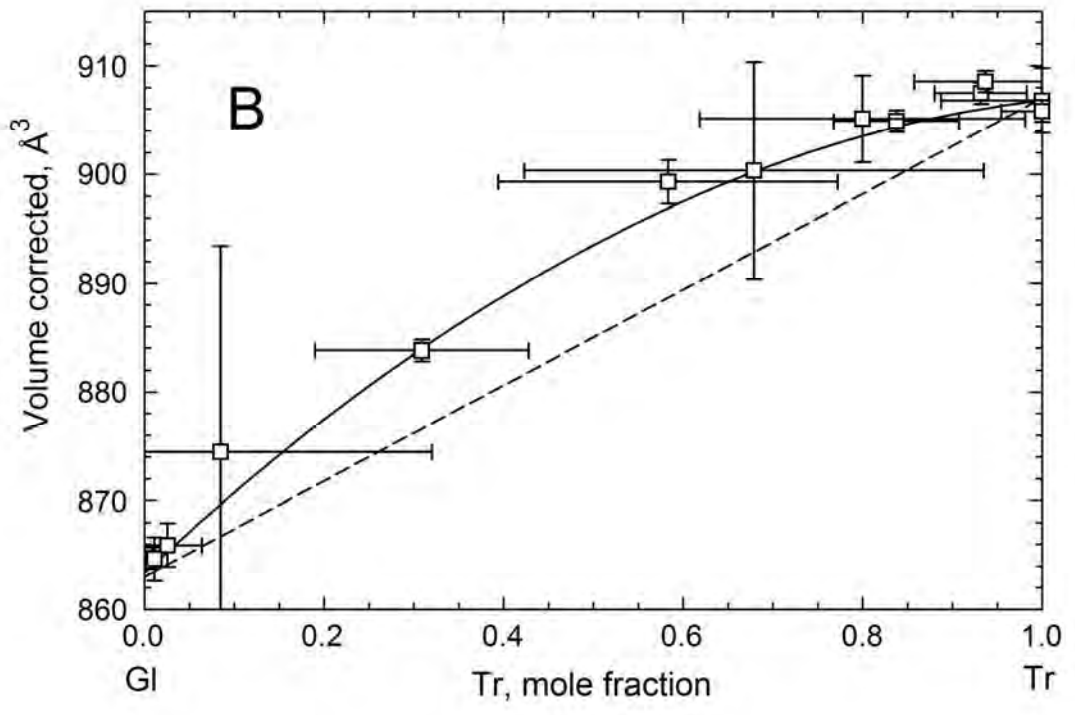

892

893

894 Figure 6.

895

896

897

898
899
900

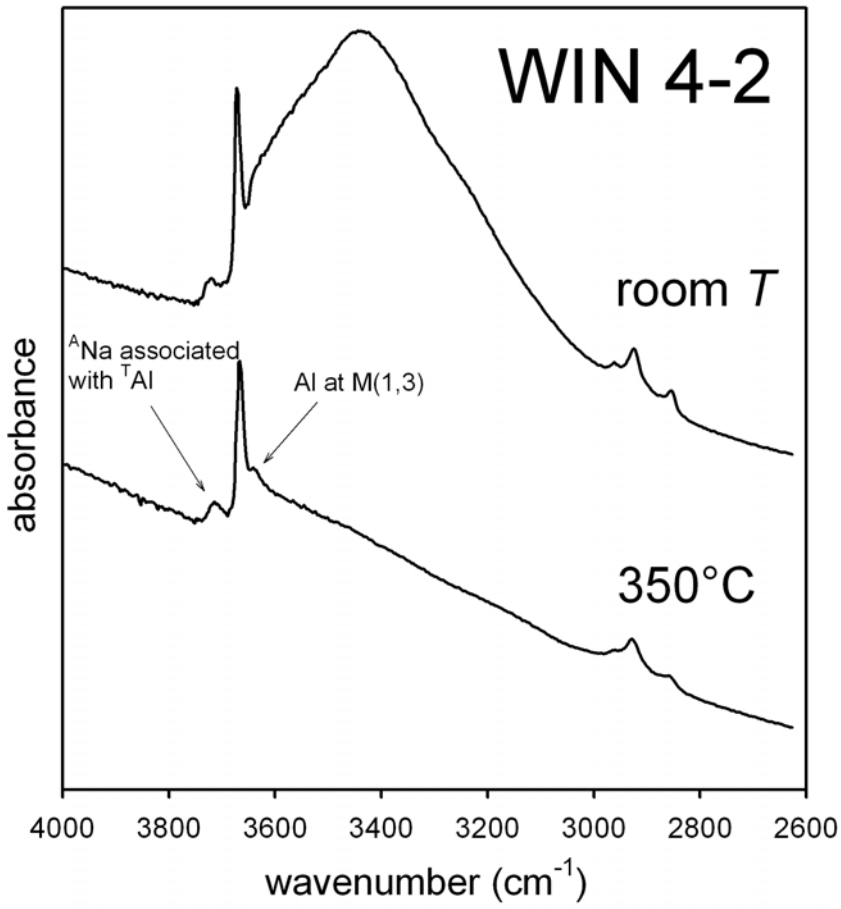

901
902
903
904
905
906
907
908
909
910
911

912
913 Figure 7a
914

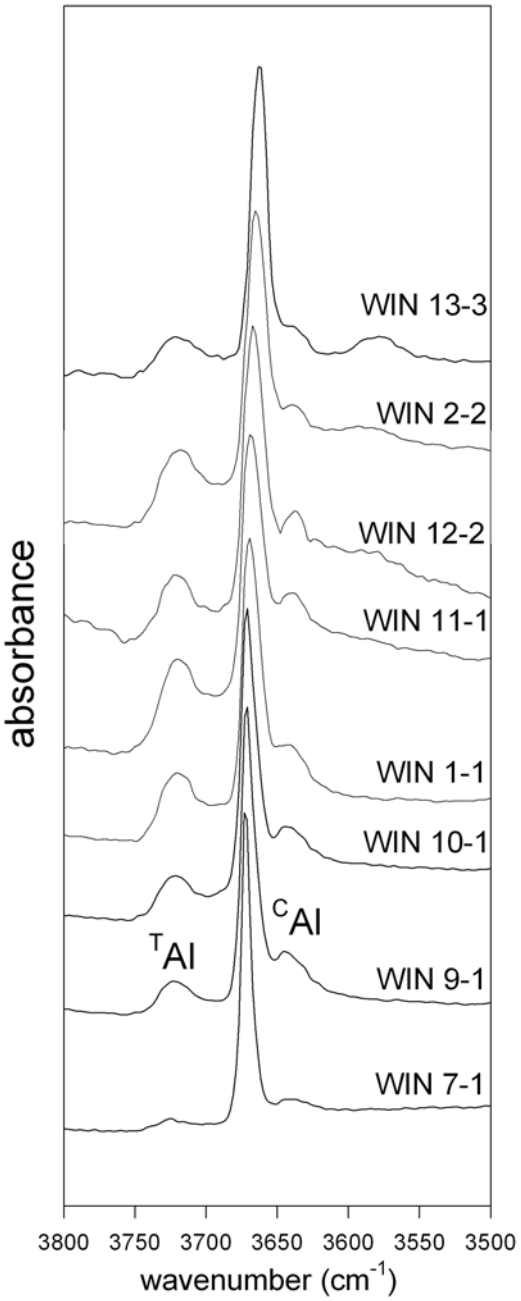

915

916

917 Figure 7b

918

919

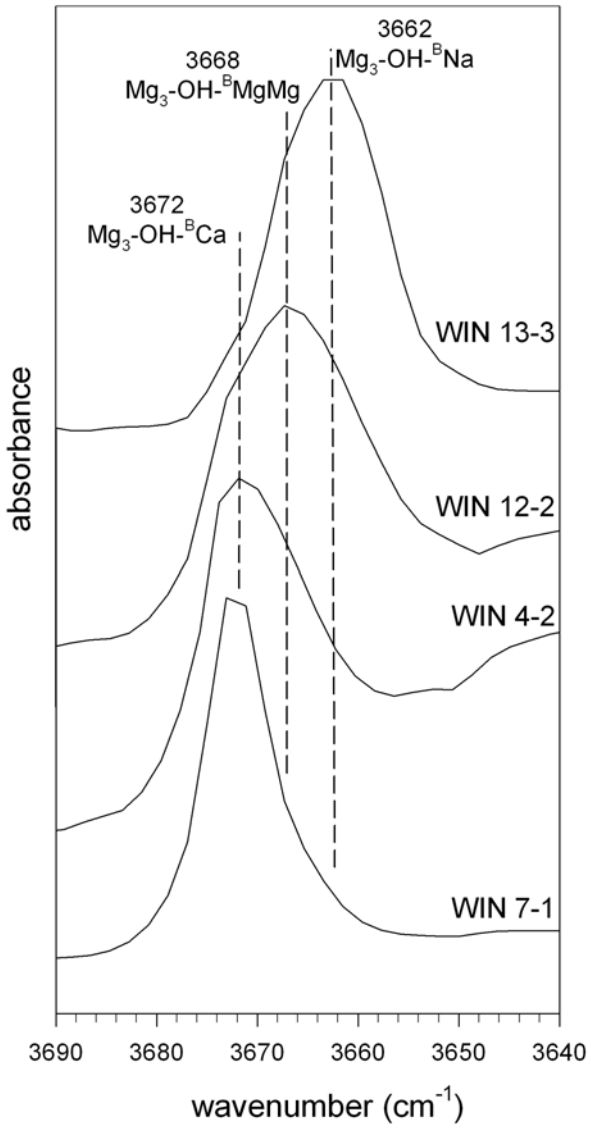

Figure 8